Diffusion Measurements of Ethane in Activated Carbon

by

PARINAZ MAKHTOUMI

A thesis submitted in partial fulfillment of the requirements for the degree of

Master of Science.

in

CHEMICAL ENGINEERING

Department of Chemical and Materials Engineering

University of Alberta

Abstract

Increasing demand for energy in the world has made industries to look for economically efficient methods to produce energy. One possible approach is to increase natural gas productions, due to its cleanliness and lower price. However, energy consumption of the cryogenic processes is high in natural gas processing plants. Adsorptive separations are becoming widespread in various industries such as oil and gas as a promising alternative to the conventional cryogenic processes. Activated carbons are among the most attractive porous materials used in adsorption processes, due to their high internal surface areas and ease of availability in the market. They exhibit bimodal pore size distributions, comprising microporous structure throughout a network of larger macropores. This makes them interesting and challenging adsorbents in adsorption studies.

The separation of ethane from natural gas is one of the important processes in gas processing plants. Ethane is highly needed as feedstock for ethylene production plants. In this thesis, adsorption kinetics of ethane on activated carbon was studied using Zero Length Column (ZLC) technique. ZLC is a useful chromatographic method to study equilibrium and kinetics of adsorption. It is known as a fast and easy lab-scale technique for adsorbent screenings and diffusion studies. In ZLC, external heat and mass transfer resistances and dispersion are eliminated by the use of low adsorbate concentration, small amount of adsorbent and high flow rates. In the experiments, the adsorbent sample is first pre-equilibrated with the test gas for a sufficient time. The kinetics and equilibrium information can be obtained from the desorption curve when the flow is switched to pure purge gas under controlled conditions.

The experimental set-up was developed during this project. System characterization experiments such as dead volume measurements, detector selection, detector's response time calculations were performed and are discussed in detail. ZLC measurements were carried out to study the controlling diffusion mechanism and obtain the diffusivity values. By performing low concentration experiments, diffusion in macropores found to be the controlling resistance. Among the various mechanisms, molecular and Knudsen diffusion were identified to be important.

To all courageous girls around the world who go beyond the traditional norms and become the leaders of their own lives.

Acknowledgements

I would first like to thank my thesis supervisor, Dr. Arvind Rajendran for his countless advice, motivation and active collaboration during this project. I am deeply grateful for giving me the opportunity to work in his research group. I broadened my knowledge and professional skills during our weekly individual and group meetings. Being a member of a multi-cultural group was a great experience. I really enjoyed our weekly group lunches and Friday evenings in the Faculty Club where we talked about movies, cultures and politics.

I acknowledge Ali and his wife who helped me to start my journey of life in Canada; I wish them a happy life together with their son Sadra. I am sincerely grateful to my colleagues, Ali and Ashwin for their help in developing the ZLC experimental set-up, and their insights through the project, Libardo who assisted me on my thesis by providing supplementary materials, Gokul, Nagesh and Nick for inviting me to their activities on the weekends. Thank you guys, it was really fun hanging out with you. I would like to also thank Adolfo, Dave, Johan, and Behnam for their support during my project. Gratitude for helping me with my work is also due to James Sawada with his guidance and advice on the experimental aspects.

I am sincerely grateful to Weizhu An for her advices on the experiments. I am also grateful to Dr. De Klerk and his student Giselle Uzcategui who helped me to conduct mercury porosimetry experiments; I wish her the best of luck in her PhD program. I would like to thank Masoud Jahandar Lashaki for his help in experimental measurement of nitrogen adsorption. I would also thank Artin Afacan, Kevin Heidebrecht and Les Dean who collaborated and helped me in this project at University of Alberta.

My thanks to Navid for patiently listening to my worries during various stages of this project, and giving me his thoughts and comments on the text of this thesis. I acknowledge Dr. Motamedi for his great contribution in reviewing my thesis and our

Sugar Bowl sessions after work in the freezing Edmonton winters. Sincere thanks to my dearest friend in Iran, Mehrnaz for her every day texts, and being there for me for almost 10 years. I would like to thank my friends in Edmonton, my roommate Sholeh for her delicious Saturday french toasts, and my friends Azadeh and Ali for their weekend's pizza nights.

Last but not least, my deepest gratitude goes to My family throughout all my endeavours. I would like to extend my gratitude onto my grandparents as well; my late grandfather for being the most unforgettable character in my life and the biggest advocate of women's education and leadership. He accompanied me in my international mathematics competition in high school which was the most memorable trip in my life.

Parinaz Makhtoumi

Contents

List of Figures

List of Tables

Nomenclature

Abbriviations

cal	Calculated by correlations
dose	Dosing cell in volumetric measurement
exp	Experimental result
sample	Sample cell in volumetric measurement

Constants

R_g	Ideal gas constant

Greek Symbols

β	ZLC dimensionless parameter
ΔU	Heat of adsorption
ϵ	Lennard-Jones constant
ϵ_p	Macropore porosity
γ	Mercury surface tension
μ	Viscosity
ρ	Density
σ	Collision diameter

τ Tortuosity

θ Contact angle of mercury and the surface

Roman Symbols

$\bar{S}$ Effective sensitivity of mass spectrometer

a Cross sectional area of adsorbate molecule, initial condition in Eq. 4.3

b Adsorption equilibrium constant for site 1, final condition in Eq. 4.3

C Concentration in the fluid phase

C_{p} Concentration in the macropores

C^* Equilibrium value of concentration in fluid phase

C_0 Initial concentration in fluid phase

d Adsorption equilibrium constant for site 2

D Diffusivity

D_{e} Effective diffusivity

D_{K} Knudsen diffusivity

D_{macro} Macropore diffusivity

D_{micro} Micropore diffusivity

D_{m} Molecular diffusivity

D_{pore} Combination of molecular, Knudsen and viscous flow diffusivities

D_{s} Surface diffusivity

D_{v} Viscous flow diffusivity

E Activation energy

F	Volumetric flow rate
H	Henry's law constant
I	Ion current
i	Intercept in V-t method
J	Mass flux
K	Effective Henry's law constant
k	Boltzman constant, Mass transfer coefficient in Eq. 2.15
k_{f}	Film resistance coefficient
L	ZLC dimensionless parameter
M	Molecular weight
m_{ads}	Mass of adsorbent
N	Avogadro Number
n	Concentration in the micropores
n_{ads}	adsorbed amount
P	Pressure
q	Adsorbed amount concentration
q_{s}	Saturation capacity
r_{c}	micropoarticle radius
R_{p}	Particle radius
r_{p}	pore radius
Re	Reynolds number

S	Detector Signal
S_{BET}	BET surface area
Sc	Schmidt number
Sh	Sherwood number
T	Temperature
V	Micropore volume
V	Volume
V_{g}	fluid phase volume
V_{s}	Skeletal volume of adsorbents
V_m	Monolayer volume adsorbed

Chapter 1

Introduction

1.1 Natural gas

Natural gas refers to the gas mixture formed from the decomposition of plants and animals under heat and pressure over millions of years. Natural gas is one of the major non-renewable fossil fuels which is commonly known as the cleanest energy among other hydrocarbon fuels [1]. According to natural gas information report in 2015 by International Energy Agency (IEA), natural gas production increased 1.6% this year compared with the production in 2014 [2] (see Fig.1.1). This jump is mostly due to an increase in natural gas productions in Iran, Qatar and the United States which are among the top natural gas producers in the world.

Canada is the fifth largest natural gas producer in the world. Natural gas resources are found in almost all the provinces and territories across Canada. Alberta is the most prominent source of fossil fuels, including natural gas, among other provinces. The first natural gas well was drilled in 1883 in southeast Alberta [3]. According to a report by Alberta government published in 2011, the remaining recoverable natural gas in this province is estimated to be 77 trillion cubic feet [tcf] [3]. The non-conventional resources are not accounted for in this estimation. They are categorized into three groups: Coal Bed Methane (CBM) is the natural gas found in coal, Shale gas is found in organic rich rocks like shale, and tight gas is trapped in low permeability rocks such as limestone. CBM and

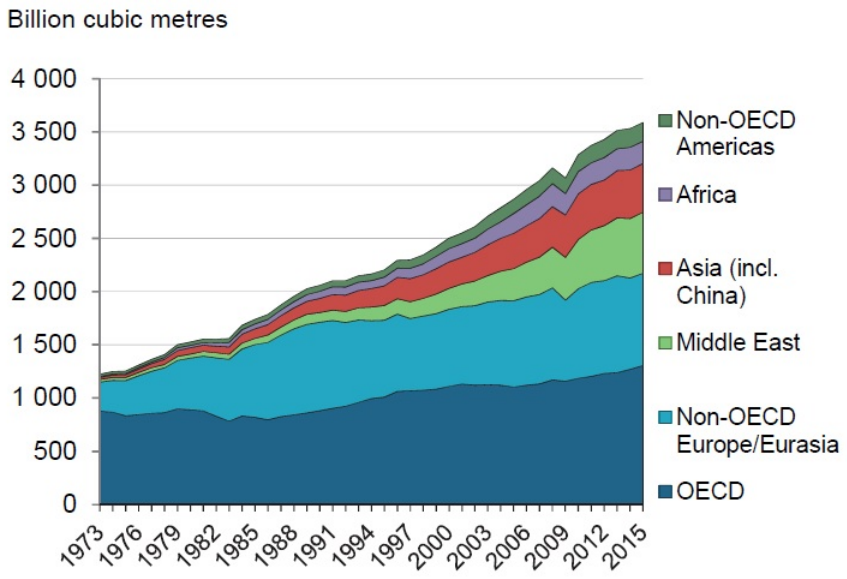

Figure 1.1: World natural gas production by region. Source: OECD/IEA Key Natural Gas Trends, IEA publishing, reproduced with permission [2].

shale gas represent approximately 8 and 0.1 percent of the total natural gas productions in Alberta in 2011, respectively. It is estimated that CBM resources in Alberta amount to about 500 [tcf]; however, the recoverable amount is still unknown. Roughly 70 percent of natural gas production in Alberta is sent to other provinces across Canada and the United States [3].

1.2 Natural gas processing

Natural gas is extensively used as fuel in industrial, commercial and residential applications. However, it consists of a different composition compared to the extracted gas. Extracted natural gas from the wells consists of hydrocarbons like methane, ethane, propane, butane, iso-butane, natural gasoline, and impurities such as water, hydrogen sulfide, carbon dioxide, helium and nitrogen [4].

In order to produce dry natural gas and satisfy pipeline quality, the extracted gas must be processed first. Natural gas processing removes impurities and separates the heavier hydrocarbons. The basic processing stages are completed in close vicinity of well-heads

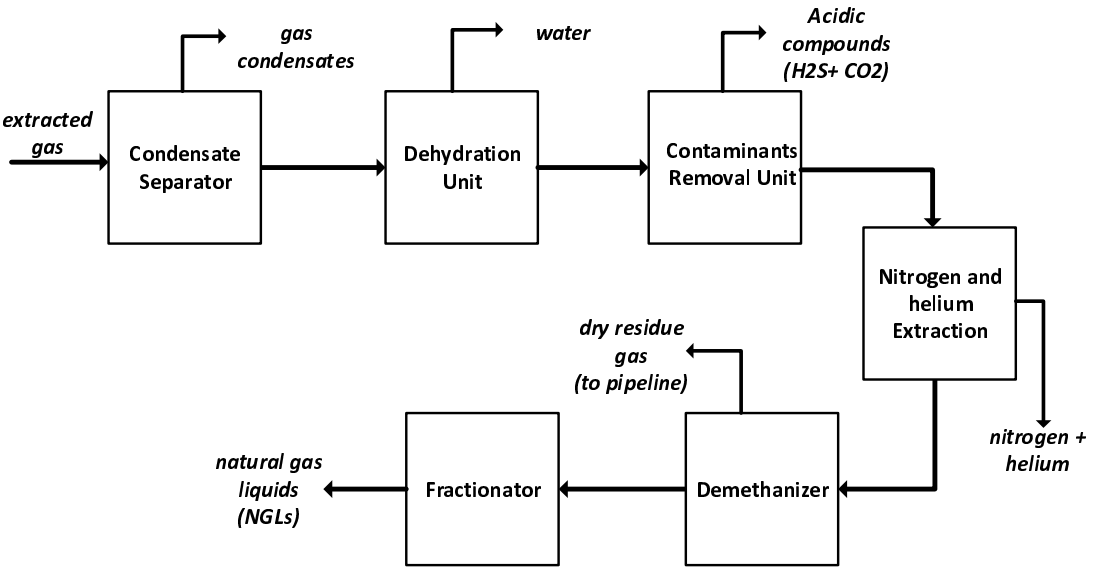

Figure 1.2: Natural gas processing unit black diagram [4].

to remove bulk amounts of water and acidic compounds [4]. The resulting stream is transported to a natural gas production plant through pipelines. The block diagram of a natural gas processing unit is shown in Fig. 1.2. According to this diagram, initially gas condensates, acidic compounds, water, nitrogen, and helium are removed from the gas. After these steps, the processed gas enters the fractionator units. Through these stages, residue gas, known as dry natural gas, is separated from the higher hydrocarbons called Natural Gas Liquids (NGL). In natural gas production plants, NGL is an important sub-product, and it is sold separately. It is used for many different areas such as enhanced oil recovery processes [5], oil refineries and petrochemical industries. The residue gas produced by demethanizer has 97% to 98% methane purity, with low concentration of ethane $(2-3\%)$. Ethane is a critical component, and it is the alternative feed for oil-based naphtha for ethylene production [6]. In the top natural gas producer countries, it is more economical to produce ethylene by ethane instead of naphtha, due to its availability and lower price [1].

The increasing demand for ethane in petrochemical industries has encouraged to study alternative energy and cost effective methods to separate ethane from natural gas [7, 8]. There have been some preliminary studies on the possibility of recovering ethane from

residue gas by adsorptive separations [9].

1.3 Adsorptive separation process

Cryogenic methods based on turbo expansion process at very low temperatures $\sim$ 188 K, are currently used to recover heavier hydrocarbons (NGLs) in natural gas processing plants. Although cryogenic units have demonstrated high efficiencies, they are neither energy nor cost efficient for medium and small applications. Adsorptive separation processes are becoming widespread in various industries such as oil and gas as a promising alternative. However, these processes have not been proven to be economically feasible. Therefore, further studies are required in this area to achieve the maximum efficiency and develop selective and durable materials.

As mentioned in the previous section, there are preliminary studies on ethane recovery from natural gas using adsorptive separation processes. Perez et al. [9] studied the separation of ethane (C_2) from residue gas using different adsorbents in a pressure/vacuum swing adsorption (PVSA) cycle by multi-objective optimization. In general, adsorption is governed by two different phenomena which take place simultaneously; equilibrium and mass transfer. In order to optimize an adsorption unit, investigations in these two areas are required. Malek and Farooq [10, 11] have performed dynamic column breakthrough experiments to obtain equilibrium and kinetics data of ethane on activated carbon and silica gel to develop a Pressure swing adsorption (PSA) simulation for hydrogen purification. There are established and reliable techniques in the literature to measure adsorption equilibrium [12]. Nevertheless, kinetics is more puzzling, due to its complexity and multiple mechanisms that occur simultaneously. As a result, detailed knowledge of gas diffusion within the porous media is needed for process design [13]. In order to study kinetics of a system the first steps are to choose a reliable experimental technique and a suitable mathematical model for correct measurements.

Mass transfer measurements by conventional uptake rate techniques are quite challenging. In these measurements, eliminating the external heat and mass transfers for strongly

adsorbed species are burdensome. In order to minimize these effects, one approach is to use small amount of adsorbent; keeping in mind that sensitivity of equipment may cause measurement limitations. In standard chromatographic measurements, external heat and mass transfers are minimized by high velocity of gas stream. The major disadvantage of this technique is the presence of axial dispersion in the system which affects the mass transfer data [12]. Zero length column (ZLC) was first introduced in 1988 by Eic and Ruthven [14] as a simple and rapid chromatographic technique to study adsorption kinetics on small samples of zeolites with no dispersion effect. The mathematical model and associated assumptions have been studied thoroughly ever since, in order to make ZLC applicable for different systems.

1.4 Activated carbon

1.4.1 Applications

Several porous materials have been studied for ethane separation processes. All these sorbents have unique characteristics, such as high capacity, thermal stability, and mechanical strength.

Activated carbons are among the most attractive porous materials used for adsorptive separation processes, due to their ease of regeneration and high diffusivities. They are known for their heterogeneous structure, randomly oriented pores, and wide pore size distribution compared to zeolites. Theses amorphous adsorbents generally show a polymodal pore size distribution. Therefore, different mass transfer mechanisms are involved in gas adsorption over these materials [15]. For this reason, adsorption kinetics in activated carbons is an interesting topic from industrial and academic point of view. Although there are several studies on adsorption of hydrocarbons over commercial adsorbents such as activated carbon, the same sample from different manufacturing companies show various kinetics behaviors. This is due to difference in the production processes and pore structure. This necessitates an independent study for every sample of activated carbon produced by any individual manufacturer.

1.4.2 Production and characteristics

Activated carbon is a term used for a wide range of materials with carbon as the core component. The common features of this group are their high porosity and high internal surface area. The production process includes combustion or decomposition of organic compounds with high carbon percentage. The first application of activated carbon was many centuries ago when Egyptians used charcoals for medical and purification applications. The first industrial use goes back to 1900 in sugar refining industry [16]. Gas adsorption by these carbonaceous materials gained attention during World War I, and was utilized in gas masks to adsorb hazardous gases. Nowadays, there are numerous types of activated carbons with versatile properties in different shapes such as granules, finely divided powders, spherical, fibrous and cloth forms. They are used in waste water treatments, air purifications, food processing and many more industries [16].

Activated carbons are composed of 85 to 95% carbon, whereas other elements such as hydrogen, nitrogen, sulfur, and oxygen are also present. These atoms exist in the raw materials, and transferred during the preparation procedure. Activated carbons are the outcome of pyrolysis of raw materials which consists of two steps; carbonization at $\sim$ 800°C, and activation by CO_2 or steam at $\sim$ 1000°C. In the first step, decomposition changes most of the noncarbon elements to volatile compounds, and others to aromatic sheets which are cross-linked randomly. The random orientation of these sheets provides free spaces that are filled with tar and other decomposition products. Activation clears the interstices, and shapes randomly distributed pores with high surface areas. The pore structure and adsorption characteristics of the carbonaceous material improves during the second step [16].

The outcome is a substance with random arrangement of microcrystallites with porous structures that are highly dependant on the raw materials and the production process. The major portion of surface area in activated carbons is present in very small pores known as micropores that have the effective diameters smaller than 2 nm. Pore classification is based on the distance between the pore walls. Micropores often have comparable

dimensions to molecules. Generally, the specific micropore volume is 0.15 to 0.7 $\frac{cm^3}{g}$ in activated carbons [13]. The surface area contributed by micropores account for roughly 95% of the total surface area. On the other hand, mesopores represent 5% of total surface area. The effective dimension of this group is 2 to 50 nm [17], with specific volume of 0.1 to 0.2 $\frac{cm^3}{g}$. Macropores are the last group in this classification, and they do not play a significant role in the adsorption process. They are the channels for gas molecules to pass through, and reach the mesopores and micropores [16]. There are different experimental methods to characterize the pore structure in porous materials. Mercury porosimetry is an effective method widely used for pore size distribution studies in the mesopores and macropore range [18]. Gas adsorption is another technique usually applied in micropore analysis [17]. These methods are covered in detail in Chapter 4.

As discussed above, the micropores provide the largest surface area and total volume in activated carbons, and play the most important role in the adsorption process. However, depending on the diffusing molecule radii, they may not enter the micropores. Similar to porous structure, chemical composition of activated carbons has a strong influence on adsorption properties. The non-carbon elements present in the activated carbon, such as oxygen and hydrogen, are located on the edges and corners of the aromatic sheets. The critical element is oxygen. Carbon-oxygen groups influence surface properties. As a result, they increase the adsorption capacity in polar systems such as water [16].

1.5 Objective and organization of the present work

As mentioned earlier, adsorptive separation processes are gaining attention in industry as an alternative technique for the conventional cryogenic processes. One of the proposed applications of adsorptive processes is separating ethane from residue gas. A detailed process design using pressure/vacuum swing adsorption on this topic has been completed in our research group [19]. One of the candidate adsorbents for this separation is activated carbon, due to its availability in the market. Hence, further investigation on adsorption of ethane in activated carbon would help to design the optimized process with high efficiency.

The aim of this work is to study diffusion behavior of ethane at low concentrations over activated carbon granules at temperatures between 303 and 373 K. In order to achieve this, Zero Length Column measurements were conducted to study the controlling mass transfer mechanism on different adsorbent sizes. Tortuosity factor is a property of adsorbent describing the pore structure of solid. This parameter is also studied carefully using the ZLC experimental results.

In this thesis, Chapter 2 reviews different mass transfer mechanisms present in adsorption, as well as related equations and the available measurement techniques. Zero Length Column fundamentals, the mathematical model, and a summary of previous ZLC studies are discussed in Chapter 3. Chapter 4 is focused on practical aspects of the present work such as experimental set-up, system characterization, experimental limitations, and solid characterization techniques, mercury porosimetry and N_2 adsorption measurements. Chapter 5 is reserved for the main ZLC experimental results, model predictions, and further discussions. Conclusion from the experimental results and recommended future work are covered in the last chapter.

Chapter 2

Diffusion in Porous Solids: Fundamentals and Measurement Methods

Solids with porous structure can accommodate large amounts of gas or liquid. This property has been utilized in several practical applications. Columns packed with these materials (adsorbents) are commonly used for removing water traces from gas or liquid streams [13]. The unique property of these materials is to selectively adsorb one component from a mixture. The same processes are implemented in oil and gas refineries to remove undesirable components. Removal of acidic compounds from natural gas can be mentioned as a notable example. Another practical application is in purification processes where increasing the purity of the valued component would result in economical advantage, e.g. oxygen purification from air for medical practices [20].

The selectivity of an adsorbent depends on the differences in either adsorption kinetics or adsorption equilibrium of the components involved in the separation [12]. As a result, studies on these two governing phenomena for each component are important, and the mechanisms should be understood carefully to model the separation behavior. The rate of adsorption is usually controlled by the fluid transport through the packed columns and inside the porous structure of the adsorbent, known as diffusion [21]. In this chapter,

different mechanisms of mass transfer in a porous solid are described, and a summary of available diffusion measurement techniques is also provided. Activated carbons are one category of the available adsorbents widely used in adsorptive processes, owing to their thermal stability and high diffusivities. Previous studies on adsorption kinetics in activated carbons is reviewed in the last section.

2.1 Diffusion

Chemical potential gradient is the driving force for any mass transport phenomena. The tendency of matter to eliminate chemical potetial variations in space and reach equilibrium is called diffusion. Diffusion takes place in all the states of matter with different rates [21]. Adolf Fick is considered the first scientist to propose a mathematical formulation to define diffusivity. He used the analogy of the Fourier heat conduction to model diffusion. Fick's first law of diffusion defines the term diffusivity resulting from concentration gradient in isothermal conditions:

$$J = -D\frac{\partial C}{\partial x} \tag{2.1}$$

In this mathematical representation, J is the mass flux, D is diffusivity, and $\frac{\partial C}{\partial x}$ is the concentration gradient. Fick's second law illustrates the concentration profile in a system where diffusion is taking place [21]:

$$\frac{\partial C}{\partial t} = D\frac{\partial^2 C}{\partial x^2} \tag{2.2}$$

Fick modeled the diffusing force in terms of concentration gradient, although it has been since established in terms of the correct form should be that of the chemical potential gradient. The simplification in using concentration gradient has consequences and are not discussed here. Readers are referred to detailed literature on this topic [21]. Since this thesis focuses on the diffusion of gases in solids only this topic will be discussed in detail.

2.2 Diffusion mechanisms

IUPAC classifies pores acording to their sizes [17]:

- pore sizes larger than $\sim$ 50 nm are called macropores;
- pore sizes between 2 nm and 50 nm are called mesopores;
- pores with sizes smaller than 2 nm are called micropores.

The diffusion mechanism depends on the pore size and the diameter of the diffusing molecules. In the large pores transport is mainly dominated by the interactions between the diffusing molecules, their collisions with the pore walls, and an additional flux due to adsorbed species. However, in sufficiently small pores, when the pore diameter is comparable with the molecular diameter, the molecules never escape from the force field of the pore walls. There are several techniques to determine the dominant diffusion mechanisms. Experiments should be conducted for each system to confirm the controlling diffusion mechanism. This section describes different possible diffusion mechanisms present in the porous materials.

2.2.1 Micropore diffusion

In micropores (pore sizes smaller than 2 nm), the pore diameter and the molecular diameter of the diffusing species are typically within the same range. The transport of diffusing molecules in these pore sizes is referred to as micropore diffusion. The practical application of this is found in size-selective separations. If the size of one species in a mixture is smaller than the micropore size of the adsorbent only that species will enter the pores. In this range, surface forces play a significant role, diffusing molecules cannot escape this strong force field, and they are considered as adsorbed phase. There are techniques available to measure micropore diffusivity, such as chromatography and NMR [12, 21] which will be discussed in detail in the next section. When diffusion in the micropores controls the rate of adsorption, the mathematical solution can be explained by Fick's first law:

$$\frac{\partial q}{\partial t} = \frac{1}{r^2}\frac{\partial}{\partial r}(r^2 D_{\text{micro}}\frac{\partial q}{\partial r}) \tag{2.3}$$

where q is the adsorbed phase concentration, r is radius vector, and D_{micro} is micropore diffusivity.

2.2.2 Macropore diffusion

If diffusion in micropores is quick enough, adsorption rate will be controlled by diffusion through the macropores and mesopores of the particle. In this case, diffusion can be controlled by four different mechanisms which are influenced by the pore size, system conditions and adsorbate properties [12]. For instance, in large pores, interactions between the diffusing molecules affect the transport rate. As pore size decreases collisions between the diffusing species and the pore walls increase. This corresponds to Knudsen diffusion. In small pores, contribution of surface diffusion becomes dominant. Total macropore diffusivity is a function of all of the controlling mechanisms combined. Pore physical properties, also, contribute to the total macropore diffusivity such as porosity and the tortuosity. Tortuosity is a geometric factor which is an intrinsic characteristic of the pores. It shows how pores deviate from an ideal cylindrical shape. Hences, it takes into account the orientation of the pores and the different pore sizes in a particle [12]. Another term which is related to the pore characteristics is the porosity (ϵ_{p}) or void space ratio in the solid particle. Both these terms can be measured using solid characterization techniques. The measurement techniques and the contribution of pore properties will be discussed in the next chapters.

The diffusivity and the equilibrium constant vary with temperature:

$$D = D_0 exp(\frac{-E}{\text{R}_\text{g} T}) \tag{2.4}$$

$$H = H_0 exp(\frac{-\Delta U_0}{\text{R}_\text{g} T}) \tag{2.5}$$

In these equations, D_0 and H_0 are the pre-exponential constants, T is temperature, R_g is the ideal gas constant, ΔU_0 and E are heat of adsorption and activation energy which are approximately within the same range. Activated diffusion mechanisms are discussed

in the subsequent sections.

Molecular diffusion

In a multicomponent mixture, when the pore diameter is large enough to neglect the molecule-wall collisions, interactions among different molecules are inevitable (See Fig. 2.1). The mathematical model of molecular diffusion in binary mixtures is presented by Chapman-Enskog [22]:

$$D_{\mathrm{m}} = \frac{0.00158T^{3/2}(1/M_1 + 1/M_2)^{1/2}}{P\sigma_{12}^2\Omega(\frac{\epsilon}{kT})} \tag{2.6}$$

In Chapman-Enskog Equation, M_1 and M_2 are the molecular weights, σ_{12} is the collision diameter from Lennard-Jones potential, ϵ is the Lennard-Jones constant, and k is Boltzmann constant. Molecular diffusivity is inversely proportional to the total pressure, and dependant on the temperature by two different terms in the nominator and the denominator of the equation. It is not dependent on gas composition. However, molecular diffusion in multicomponent mixtures becomes composition dependent.

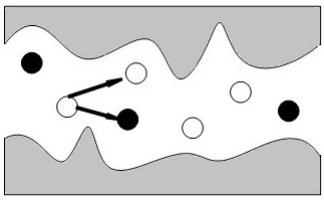

Figure 2.1: Schematic description of molecular diffusion inside the macropores. Diagram is not scaled.

Knudsen diffusion

In small macropores, the molecule-wall collisions occur more frequently than collisions among the molecules. This phenomenon, known as Knudsen diffusion, controls the diffusion in the small pores or at low gas concentrations. A qualitative description of Knudsen diffusion is shown in Fig. 2.2. When a molecule hits the pore wall, it gets adsorbed on the surface and released instantly. Therefore, the velocity of the molecule is not a

function of its initial velocity, and its direction is random [21]. When Knudsen is the controlling mechanism, each component diffuses individually; therefore, composition is not a contributing factor. Knudsen diffusion is defined by:

$$D_{\mathrm{K}} = 97 r_{\mathrm{p}} \sqrt{\frac{T}{M}} \tag{2.7}$$

In this equation, M is the molecular weight of the diffusing molecules, r_{p} is the pore radius, and T is the system temperature. Knudsen diffusion depends on the square root of temperature and is not affected by the pressure or the total concentration [12].

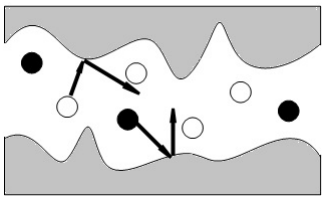

Figure 2.2: Schematic description of Knudsen diffusion inside the macropores.

Viscous flow

In a system where there is a pressure difference across the pores, the resulting laminar flow adds an additional flux to the total diffusivity (See Fig. 2.3). If the pressure gradient across the particle is very small, the diffusion flux due to viscous flow is negligible. This type of diffusivity is calculated by:

$$D_{\mathrm{v}} = \frac{P {r_{\mathrm{p}}}^2}{8\mu} \tag{2.8}$$

in which μ is the gas viscosity in [poise], r_{p} is the pore radius in [cm], and P is the total pressure in $[\frac{dynes}{cm^2}]$ [12].

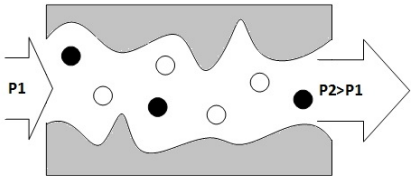

Figure 2.3: Schematic description of viscous flow diffusion inside the macropores.

Surface diffusion

In the situation where adsorbed phase concentration on the solid surface is significant, an additional flux, due to transport of adsorbed species on the surface is probable, this phenomenon is called surface diffusion. Fig. 2.4 demonstrates the presence of this additional flux on the solid surface schematically. Surface diffusion is strongly concentration dependant, so it becomes important when the adsorbed thickness is considerable [12]. At high temperatures, this additional flux is less, due to decreased adsorbed phase concentration. All the three macropore mechanisms described earlier take place inside the pores; however, surface diffusion occurs on the solid surface in parallel. Therefore, surface diffusivity is additive to pore diffusivity; the combined term is expressed as:

$$D_{\text{macro}} = D_{\text{pore}} + K(\frac{1-\epsilon_{\text{p}}}{\epsilon_{\text{p}}})D_{\text{s}} \tag{2.9}$$

in this equation, D_{pore} is the combined pore diffusivity from molecular, Knudsen and viscous flow diffusivities, and D_{s} is the surface diffusivity, K is dimensionless effective Henry's constant based on the solid volume, and ϵ_{p} is the particle porosity [21].

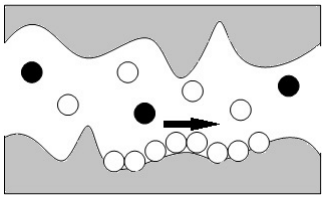

Figure 2.4: Schematic description of surface diffusion inside the macropores

In macropores, when both molecular and Knudsen diffusions are significant in the system, the combined diffusivity is calculated using the same expression as electrical resistances in series. If there is an additional flux due to surface and viscous flow diffusions in the system they will be added to the combined diffusivity; they behave like paralllel resistances [21], the correlation is given by:

$$D_{\text{macro}} = \frac{1}{\frac{1}{D_{\text{m}}} + \frac{1}{D_{\text{K}}}} + D_{\text{v}} + K(\frac{1-\epsilon_{\text{p}}}{\epsilon_{\text{p}}})D_{\text{s}} \tag{2.10}$$

2.3 Mass transfer resistances

The adsorption of a component is usually described by two transport mechanisms; transport through the gas medium to the surface of the adsorbent, and transport into the particle known as diffusion. The combination of these mechanisms control the rate of adsorption. Transport inside the porous particles was discussed in the previous section, the particle is typically surrounded by a laminar layer, and mass transfer occurs from this sub-layer to the particle surface by molecular diffusion. Film resistance can be defined by the linear driving force (LDF) equation:

$$\frac{\partial \bar{q}}{\partial t} = \frac{3k_{\mathrm{f}}}{R_{\mathrm{p}}}(C - C^{*}) \tag{2.11}$$

In this equation, $\bar{q}$ is the average adsorbed phase concentration over the particle, R_{p} is the particle radius, C is the concentration of the diffusing molecules, and C^{*} is the fluid phase concentration that would be at equilibrium with the adsorbed phase. Mass transfer coefficient introduces a dimensionless parameter called Sherwood number (Sh) which is defined by:

$$Sh = \frac{2k_f R_p}{D_m} \tag{2.12}$$

This number in the analogous to Nusselt number (Nu) in heat transfer studies. In the static conditions Sherwood number is equal to 2.0. It increases with an increase in the flow. The sherwood number is related to Reynolds (Re) and Schmidt (Sc) numbers which are the dimensionless parameters characterizing the flow conditions [21]. There are several correlations that show the relationship between these three parameters in solid-fluid systems as found in the literature [22]. One such correlation is [12]:

$$Sh = 2.0 + 1.1Sc^{\frac{1}{3}}Re^{0.6} \tag{2.13}$$

Transport inside the pores is typically slower than transport through the external fluid film. As a result, the fluid film usually has a minor contribution in the total resistance

as compared to pore diffusion mechanisms. If more than one resistance control the mass transfer in the system, the effective mass transfer coefficient k is defined as [12]:

$$\frac{1}{kH} = \frac{{r_c}^2}{15HD_{\text{micro}}} + \frac{{R_p}^2}{15\epsilon_p D_{\text{macro}}} + \frac{R_p}{3k_f} \tag{2.14}$$

In this equation, H is equilibrium constant, r_c is micro-particle radius, and R_p is particle radius.

2.4 Experimental techniques

There are several available techniques to study diffusion in porous materials. This section contains a brief review of the traditional methods used for studying adsorption kinetics.

2.4.1 Uptake rate measurements

One of the techniques commonly used for determining the intraparticle diffusivity is batch experiment. In this technique, a number of particles are placed in the apparatus, and are exposed to a step change in sorbate concentration at the external surface of the particle at time zero. The rate of adsorption is measured by following the mass of the adsorbent (gravimetry) or the pressure in the chamber (volumetry). The diffusional time constant can be calculated by comparing the experimental results to the analytical solution. The particles used in the experiment can be either adsorbent crystals or pellets. This measurement requires a very sensitive balance or pressure transducers for reliable results [12].

Although straightforward this technique has a few shortcomings. The use of large mass of the solid leads to strong heat effects that can mask the measurement of mass transfer.

2.4.2 Chromatographic methods

The external heat and mass transfers cannot be perfectly eliminated in the batch experiments. Chromatographic methods are the alternative to the conventional uptake rate measurements. In these methods, a gas stream flows through a column packed with the

adsorbent particles. Chromatographic measurements are performed by a step change or pulse injection to a packed column, or a reduced amount of adsorbent particles, called differential beds. Dispersion may be present in such systems. In order to separate the dispersion and mass transfer effects, experiments over a range of gas velocities should be performed [12].

One of the chromatographic techniques in which experiments are carried out on a small amount of adsorbent under high flow rates of gas is Zero Length Column (ZLC) [14]. It was developed to study intraparticle diffusivities by eliminating the dispersion effect which is present in other chromatographic techniques [21]. Zero Length Column is the method used for diffusion measurements in the present study and will be discussed in the following chapter.

2.4.3 NMR spectroscopy

Nuclear magnetic resonance (NMR) spectroscopy is an analytical technique widely used in organic chemistry to detect the unknown species in complex solutions. This technique was developed based on the interactions between the diffusing molecules in an external magnetic field. It is also used in characterising atoms and molecules in order to determine the diffusivity and solubility. This method is a powerful technique for diffusion measurements such as elementary processes in the molecular level. Self diffusion measurements is another application where the molecules under study are labeled and experiments are performed under equilibrium condition [21]. However, this technique is more suitable in molecular and self diffusivity determination.

2.5 Diffusion in activated carbon

Activated carbons are widely used in adsorptive separation processes [23]. They are commercially available in large amounts, and they possess unique properties relevant to these processes, such as high internal surface area, thermal staibility and high diffusion rates [24]. According to their pore analysis, they have randomly ordered pore network

with wide pore size distributions, due to their production procedure [13]. They exhibit bimodal distributions, comprising microporous structure throughout a network of larger macropores. Therefore, diffusion in such systems is more complex than similar systems [21]. As mentioned earlier, adsorption of gas on adsorbent particles is controlled by various mass transfer resistances; transport to the particle surface and diffusion into the particle. Film resistance can be determined by the relevant equations available in the literature [22]. On the other hand, the rate of diffusion of the gas in the adsorbent particle should be measured and calculated for each system with the aid of mathematical models [25].

Gas diffusion in the macropores is usually due to molecular and Knudsen diffusions. In activated carbons, it is possible for gas molecules to adsorb significantly on the surface. This adds an additional flux in parallel to that of the pore diffusion, and accelerates the transfer [26]. This mechanism is known as surface diffusion, and is significant at high adsorbed concentrations. Doong et al. [27] studied PSA separation of a mixture of CO_2, H_2, and CH_4, and noticed that surface diffusion contributed 50% of the total flux over the activated carbon sample. Do et al. [28] perfromed differntial adsorption bed (DAB) experiments of ethane in activated carbon. They proposed a model based on pore and surface diffusion in the system. They could successfully verify the model by the DAB results. Unlike pore diffusion, surface diffusion is concentration dependant; i.e. adsorbed molecules become more mobile in higher concentrations. There are available models that describe the concentration dependence of surface diffusion of different species on activated carbons [29, 30]. The classical theories used for surface diffusion cannot be applied for activatd carbon. Mesured surface diffusivities in activated carbons have been shown faster behavior. This behavior is due to the disordered distribution of pores in their structure [31]. Hu et al. [32] performed DAB experiments of ethane and propane in Ajax activated carbon differentially in order to study the concentration dependence of surface diffusion. They observed that at higher surface coverages, the traditional theories fail to explain high surface diffusivities in activated carbons. Micropore diffusion was also predicted and observed by the previous studies in the small and medium size particles of activated carbon. Hu and Do [33], developed a mathematical model for adsorption of

hydrocarbons in small particles of activated carbons. They showed that ethane adsorption on activated carbons is not only controlled by macropore diffusion but also micropore diffusion, and the combination of pore and surface diffusions cannot fully predict the uptake rate results.

Mayfield and Do [15] used an activated carbon sample which showed a bimodal pore size distribution (see Fig. 2.5). They described mass transfer in a single particle of Ajax activated carbon with a mathematical model where macropore, surface and micropore diffusions were contributing to the total mass transfer. At higher temperatures, as the adsorbed phase concentration decreases, surface diffusion drops significantly [29]. Therefore, mass transfer in adsorbent pellets is only controlled by gas-phase macropore diffusion. Mayfield and Do [15] utilized this feature in order to predict the tortuosity (τ_{M}) of their sample.

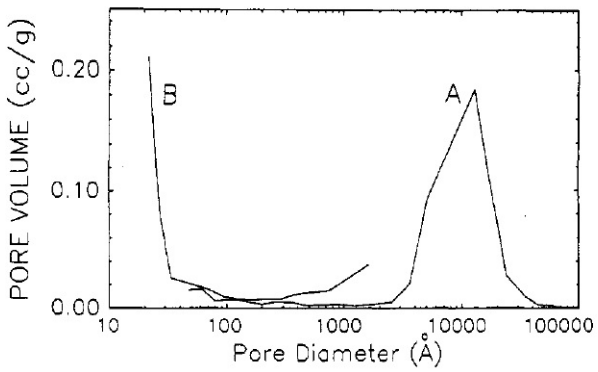

Figure 2.5: Pore size distribution of Ajax activated carbon from mercury porosimetry and nitrogen adsorption by Mayfield et al. [15]- reproduced with permission from ACS Publications

Chapter 3

Zero Length Column Technique

Zero length column (ZLC) is one of the available techniques to study diffusion. It was first introduced by Eic and Ruthven to measure intracystalline diffusivity in zeolite powders [14]. Over these years, the method has been extended and modified to measure diffusion in pellets, liquid systems, bi-porous materials, and to study equilibrium. The advantage of this approach lies in the elimination of external heat and mass transfer resistances by using small amount of adsorbent, low concentration of sorbate in gas, and high flow rates of purge gas. In comparison with the conventional chromatographic methods, ZLC is simple and fast which makes it a suitable candidate for lab-scale adsorption kinetics studies or rapid screenings [34,35]. The diffusion measurements reported in this thesis were all performed using ZLC technique. This chapter is focused on ZLC background, theory and the previous studies on this topic.

3.1 Theory of ZLC

In ZLC, the column is packed with a small amount of the adsorbent ($\sim$ 5 mg). The sample is first pre-equilibrated with the test gas. Then, a switching valve is used to switch the gas stream from the test to a non adsorbing purge gas, typically helium. Kinetics and equilibrium characteristics of the system are measured by following the desorption behavior of the adsorbate. The mathematical model used to describe the ZLC

system, is based on the Fick's second law of diffusion describing the mass balance in the particles [21]. In addition, mass balance of the adsorbing component in the fluid phase is, also, considered. These two mass balances have to be solved simultaneously, to derive the desorption curve. In this model it is assumed that system is at isothermal conditions, particles are spherical, and ZLC column is a well mixed cell [14]. It is worth noting that account for these deviations have also been proposed in the literature [36, 37]. Figure 3.1 shows a schematic diagram of ZLC column as a CSTR. In this figure, particle was first exposed to the test gas, and desorption is followed by the outlet concentration. Under these conditions, the differential mass balance in the fluid phase is:

$$V_{\mathrm{s}}\frac{d\bar{q}}{dt} + V_{\mathrm{g}}\frac{dC}{dt} + FC = 0 \tag{3.1}$$

where V_{s} is the volume of the particle, $\bar{q}$ is the average concentration of adsorbate in the particle, V_{g} is the fluid phase volume, known as dead volume of the system, C is the concentration of adsorbing component in the fluid phase, and F is volumetric flow rate of the purge gas.

The mass balance in the macropores is described by:

$$(1-\epsilon_{\mathrm{p}})\frac{\partial \bar{n}}{\partial t} + \epsilon_{\mathrm{p}}\frac{\partial C_{\mathrm{p}}}{\partial t} = \frac{\epsilon_{\mathrm{p}}}{\tau} D_{\mathrm{macro}}\left(\frac{\partial^2 C_{\mathrm{p}}}{\partial R^2} + \frac{2}{R}\frac{\partial C_{\mathrm{p}}}{\partial R}\right) \tag{3.2}$$

where ϵ_{p} is porosity of the particle, $\bar{n}$ is average concentration of adsorbate in the micropores, τ is tortuosity of the particle, C_{p}, is the concentration of adsorbate in the macorpores, and D_{macro} is macropore diffusivity. The mass balance in the micropores is given by:

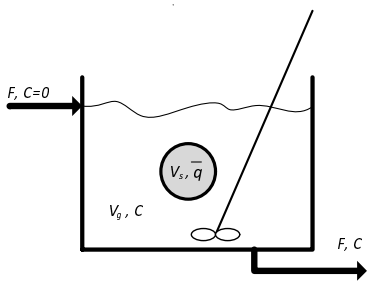

Figure 3.1: Schematic Description of ZLC column as a CSTR.

$$\frac{\partial n}{\partial t} = D_{\text{micro}} \left(\frac{\partial^2 n}{\partial r^2} + \frac{2}{r} \frac{\partial n}{\partial r} \right) \tag{3.3}$$

$$\frac{\partial \bar{n}}{\partial t} = \frac{3}{r_{\text{c}}} D_{\text{micro}} \frac{\partial n}{\partial r}\Big|_{r=r_{\text{c}}} \tag{3.4}$$

$$\frac{\partial \bar{q}}{\partial t} = \frac{3}{R_{\text{p}}} \frac{\epsilon_{\text{p}}}{\tau} D_{\text{macro}} \frac{\partial C_{\text{p}}}{\partial R}\Big|_{R=R_{\text{p}}} \tag{3.5}$$

In the equations above, D_{micro} is micropore diffusivity, and r and R corresponds to radius vector in adsorbent micro-particles and particle respectively. If the adsorbed phase in the micropores is at equilibrium with the gas in the macropores, by assuming Henry's law $\bar{n} = HC_p$, particle mass balance, Eq.(3.2) reduces to:

$$[(1-\epsilon_{\text{p}})H + \epsilon_{\text{p}}] \frac{\partial C_{\text{p}}}{\partial t} = \frac{\epsilon_{\text{p}}}{\tau} D_{\text{macro}} \left(\frac{\partial^2 C_{\text{p}}}{\partial R^2} + \frac{2}{R} \frac{\partial C_{\text{p}}}{\partial R} \right) \tag{3.6}$$

Therefore, the effective macropore diffusivity is defined by:

$$D_{\text{e}} = \frac{\epsilon_{\text{p}}}{\tau} \frac{D_{\text{macro}}}{[(1-\epsilon_{\text{p}})H + \epsilon_{\text{p}}]} \tag{3.7}$$

If mass trasfer is controlled by diffusion in both macropores and micropores, the two mass balance equations for each controlling transport should be written and solved simultaneously [21]. In order to solve the system of differential equations for the gas phase concentration, suitable initial and boundary conditions are required and are provided below.

- Initial conditions: $C_p(0, R) = C_i$
- Boundary condition: $\frac{\partial C_p}{\partial R}\big|_{R=0} = 0$

Therefore, solution to the diffusion model yields [14]:

$$\frac{C}{C_0} = 2L \sum_{n=1}^{\infty} \frac{\exp(\frac{-\beta_n^2 Dt}{R^2})}{[\beta_n^2 + (L-1)L]} \tag{3.8}$$

$$\beta_n \cot \beta_n + L - 1 = 0 \tag{3.9}$$

$$L = \frac{1}{3}\frac{F}{KV_s}\frac{R^2}{D} \tag{3.10}$$

$$K = (1 - \epsilon_{\mathrm{p}})H + \epsilon_{\mathrm{p}} \tag{3.11}$$

where K is the dimensionless effective Henry's constant which is related to Henry's constant by Eq. 3.11, β_n are the positive roots of Eq. 3.9, L is a dimensionless parameter which introduces purge flow rate into the equations. If the mass transfer in the system is controlled by diffusion in micropores, the term $\frac{D}{R^2}$ in the above equations would be replaced by $\frac{D_{\mathrm{micro}}}{r_{\mathrm{c}}{}^2}$. On the other hand, if the controlling resistance is present in the macropores, then, $\frac{D}{R^2}$ can be replaced by $\frac{D_{\mathrm{e}}}{R_{\mathrm{p}}{}^2}$. L represents the ratio of convective flux to diffusive flux [38]. At low flow rates ($L < 1$) or large sample mass, the adsorbate would have enough time to reach equilibrium with the purge stream. In this scenario, desorption rate would be controlled by convection, and it is reasonable to assume that the solid and the gas would always be at equilibrium. Thus, the Henry's constant can be calculated by desorption curve. However at sufficiently high flow rates ($L > 10$), the desorption rate would be controlled by diffusion of sorbate out of particle. Under these conditions, the ZLC response curve yields both Henry's constant and the diffusional time constant [39]. In other words, if the primary aim is to obtain kinetics information, the experiment should be carried out at ($L > 10$).

From the analysis, it is clear that the ZLC might fail in strongly adsorbed systems. In these cases, it may be difficult to find the flow rate that yields to high L values, with sufficient fluid concentrations that can be monitored accurately. It is noteworthy to mention that the system diffusion time should be greater than the response time of the detector as well as the dead volume. This indicates a maximum limit that ZLC is applicable for the given particle or crystal size. The main advantage of ZLC is elimination of external mass transfers and axial dispersion. The absence of these external resistances can be varified by changing the sample mass and the purge flow rate [12].

3.2 Long time asymptote analysis

As mentioned above, there are two different regimes that can control the ZLC desorption experiments. In non-equilibrium conditions when diffusion controls desorption of adsorbate, the mathematical solution will be Eq. (3.8). At higher t values, only the first term of the summation is significant [14], and the solution simplifies to [14]:

$$\frac{C}{C_0} = \frac{2L}{[\beta_1^2 + (L-1)L]} \exp(\frac{-\beta_1^2 D}{R^2} t) \tag{3.12}$$

As per above equation, for longer periods, the ZLC response curve yields a straight line on a semi-logarithmic plot of the normalized concentration versus time. At large L values (> 10), β_1 approaches π. In the solution, knowing the sample mass, density, and the particle radius, the effective diffusivity and the Henry's constant can be determined using the slope, $(\frac{-\pi^2 D}{R^2})$, and the intercept, $(\ln(\frac{2L}{[\pi^2+(L-1)L]}))$, of the asymptote.

3.3 Equilibrium control

More accurate estimation of K (dimensionless effective Henry's constant) can be obtained from experiments at low flow rates ($L < 1$) [40, 41]. If interest is to measure diffusivity, this regime should be avoided. At these conditions, desorption occurs by convection under equilibrium rather than diffusion out of particle. ZLC equilibrium measurements can be used for material ranking purposes based on equilibrium capacity [35]. Under assumption of linear equilibrium between the adsorbed phase and gas phase concentrations, the mass balance equation provides a simple exponential form:

$$\frac{C}{C_0} = \exp(\frac{-Ft}{KV_s + V_g}) \tag{3.13}$$

A plot of $\ln(\frac{C}{C_0})$ versus t yields a straight line through the origin, and the Henry's constant can be obtained directly from the slope [38]. For strongly adsorbed species, the dead volume of the system (V_g) can be neglected, due to high values of equilibrium constant. However, for weakly adsorbed species, both terms in the denominator are in the same

order of magnitude. In this case, V_g can be easily measured by the same ZLC experiment with an empty column. The area under the ZLC blank response curve provides the dead volume of the system. In an equilibrium controlled system, the ZLC desorption curve in the plot of $\frac{C}{C_0}$ versus Ft (Flow $\times$ time) only depends on the desorption volume [39]. This indicates that the curves at different flow rates should overlap. On the other hand, in a kinetically controlled system, curves would diverage. An increase in the flow rate results a decrease in the fluid phase concentration. There is a point at which ZLC response for higher flow rate crosses the lower flow rate response. These are the simple experimental checks to confirm whether experiments are performed under equilibrium or the kinetically limited conditions [42]. Figure 3.2 shows qualitative desorption curves and Ft plot for a gaseous system at three different flow rates (L values). As the flow rate increases, the ZLC response deviates from the linear form, which confirms non-equilibrium conditions. In addition, the cross points on the Ft plot for higher flow rates are clearly noticeable.

For more concentrated systems, the isotherm may be described by suitable isotherm models. Therefore, Eq. (3.14) should be substituted in the mass balance equation where

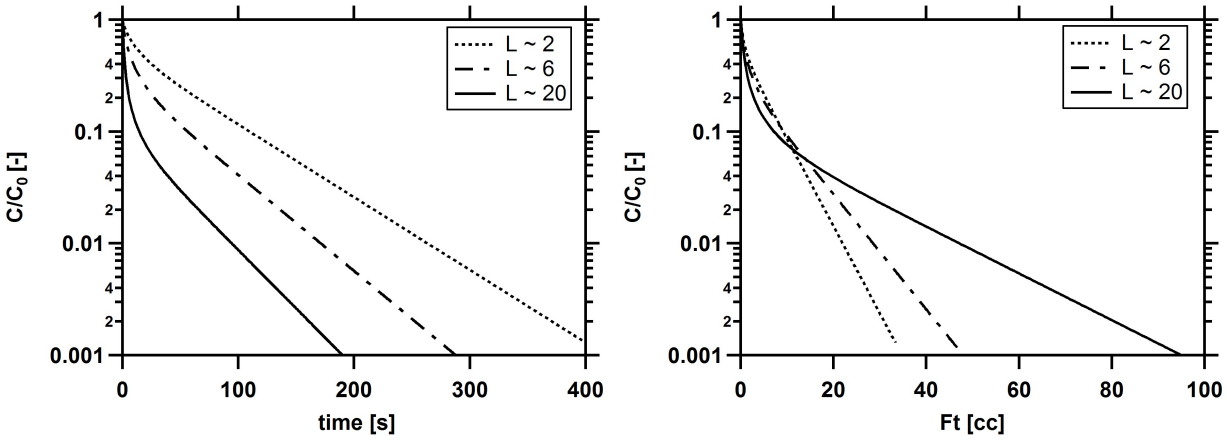

(a) (b)

Figure 3.2: (a) ZLC desorption curves for a gaseous system, and (b) corresponding Ft plot for a kinetically controlled experiments. Different L values are equivalent to different flow rates.

$\frac{dq}{dC}$ is calculated by the isotherm model. For a system modelled by Langmuir isotherm, the solution of the ZLC desorption curve under equilibrium conditions will be characterized as Eq. (3.15) [38].

$$\frac{dq}{dt} = \frac{dq}{dC}.\frac{dC}{dt} \tag{3.14}$$

$$\ln(\frac{C}{C_0}) = \frac{-Ft}{KV_s + V_g} - \frac{KV_s}{KV_s + V_g}\left[\frac{1}{1+bC} - \frac{1}{1+bC_0} + \ln(\frac{1+bC_0}{1+bC})\right] \tag{3.15}$$

This solution reduces to a linear response at very low concentrations.

3.4 Previous studies using ZLC

Since the time ZLC was introduced to determine diffusivity of gases in microporous solids [14], it has been applied to several systems, in order to measure and obtain the controlling diffusion mechanims: intracrystalline (micropore) diffusion, macropore diffusion [39, 43], and surface resistance [44]. Through the time, the method has been changed and modified to study self diffusivity [45], counter diffusion [46], kinetics in liquid systems [46]. These modifications change the traditional ZLC to be applicable under non-linear conditions [47], non-isothermal systems [48], biporous adsorbents [49]. In addition, Brandani et al. [40,41] modified the ZLC assumptions to measure equilibrium for single components and binary systems which was explained in detail in the previous section. Table 3.1 lists some of previous works on ZLC and case studies.

Table 3.1: Limited set of previous ZLC studies

Adsorbate	Adsorbent	Case study	Citation
o-xylene	50 and 100 micron NaX	micropore diffusion	Eic and Ruthven (1988) [14]
O_2, N_2	5A pellets	macropore diffusion	Ruthven and Xu (1993) [43]
benzene, n-hexane	13X	counter diffusion	Ruthven and Stapleton (1993) [46]
benzene, hexane	NaX crystals	liquid system	Brandani and Ruthven (1995) [50]
methanol	NaX crystals	self diffusion	Brandani and Ruthven (1995) [45]
benzene and p-xylene	silicalite	non- linear condition	Brandani et al. (2000) [51]
CO_2	CaA, NaLSX	single component equilibrium	Brandani et al. (2003) [40]
CO_2/C_2H_4 and CO_2/C_3H_8	NaLSX, NaX, CaX, and CaA	binary systems equilibrium	Brandani and Ruthven (2003) [41]
CH_4	DDR zeolite	micropore diffusion and surface resistance	Vidoni et al. (2012) [44]
CO_2, CH_4	binderless 13X beads	micropore diffusion	Silva et al. (2012) [52]

Chapter 4

Experimental Procedure and Solid Characterization

In the previous chapter, we discussed that the ZLC technique was modified to study kinetics and equilibrium in different systems. The mathematical model based on Fick's law of diffusion was provided. In this chapter, details of the ZLC experiments such as experimental set-up and procedure, choice of detector, data processing method, dead volume measurements, and solid characterization experiments are discussed.

4.1 ZLC set-up

During this project, a ZLC set-up was developed to study diffusion in porous solids. Some preliminary tests on the set-up and the solid were conducted prior to the ZLC experiments, such as dead volume determination and solid characterization. These aspects will be discussed in the following sections. Figure 4.1 shows the schematic diagram of the ZLC set-up. Alicat MC series flow controllers were placed on each line, controlled and monitored with OPTO-22 and LabView interface. The minimum and maximum controllable flow rates of the Alicat flow controllers were respectively, 1 and 500 sccm.

The zero length column in the ZLC experiments, was a 1/8" to 1/16" Swagelok reducer (4.2). The particles were placed on top of 100 μm mesh which was used for holding them

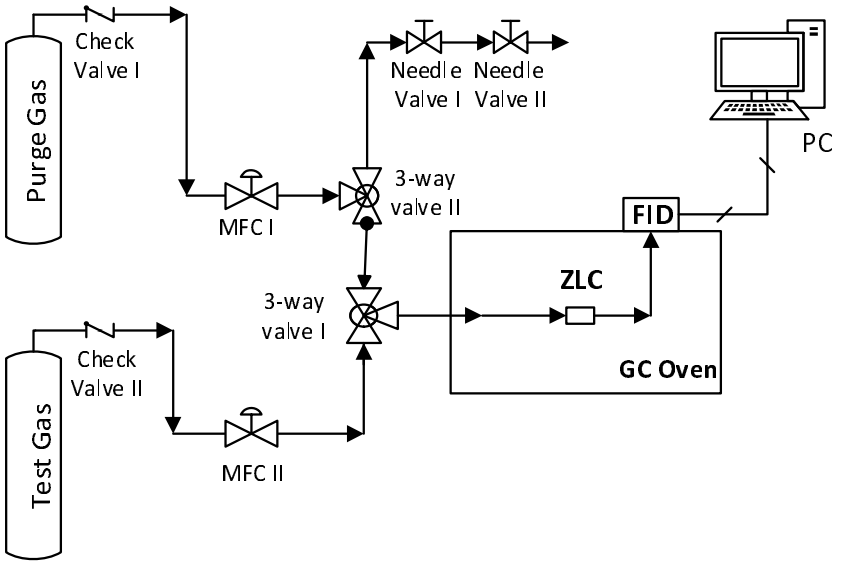

Figure 4.1: Schematic diagram of the ZLC experimental set-up used in this work.

in one end of the reducer. Schematic diagram of the column is shown in Fig. 4.2. The cell was placed in the GC oven (HP 5890) for in-situ sample activation. The outlet of the cell was connected to a Flame Ionization Detector (FID), in order to monitor the concentration of the effluent gas. FIDs are sensitive detectors, widely used for organic species in gas chromatography. The ZLC response curves were recorded in the computer for further data analysis.

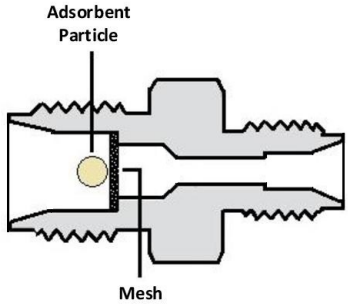

Figure 4.2: Zero length column, Swagelok 1/8" to 1/16" reducer with one particle in one end.

In all the experiments, 2-GA activated carbon obtained from Kuraray corporation was used. Prior to the experiments, the sample was activated at 200°C for a particle of ~ 4 mg at the flow rate of 5 sccm. The test was dry dilute ethane, 1% ethane mixed with helium, as provided by Praxair. In the experiments both He (purity of 99.5%) and N_2 (purity of 99.5%) provided by the same company was used as the purge gas.

4.2 ZLC procedure

The ZLC experiments were started by regenerating the adsorbent by subjecting it to high temperature. After activation, the system temperature was reduced to the experimental temperature (30, 50 or 70°C), and the sample was pre-equilibrated with the test gas (helium stream containing 1% ethane) for a period of 1 hour. At time zero, the flow was switched to pure purge gas (He or N_2) at the same flow rate. In order to have a smooth transition when switching the valve, a vent line was added to the purge line prior to the main switch valve. Two needle valves were installed on the vent line to maintain the system pressure at a constant value. The FID signal was continuously monitored by computer, and then converted to normalized concentration. The ZLC tests were performed at different flow rates ranging from 5 to 50 sccm, and were repeated to ensure data reproducibility.

4.3 Choice of detector

ZLC experiments require a sensitive detector to monitor the concentration of the sorbate in the gas stream. In order to find the best detector for the system under study, preliminary tests on different detectors namely, Flame Ionization Detector (FID), Thermal Conductivity Detector (TCD), Mass Spectrometer (MS) were studied and tested for accuracy, sensitivity, ease of calibration and dead volume.

Flame ionization detector (FID)

Flame ionization detectors are widely used in organic gas chromatography and are well-known for their sensitivity. In this type of detector, the gas passes through a hydrogen/air flame, and combustion of the gas in the flame produces ions. The generation of the ions is proportional to the concentration of organic species in the gas stream. The main disadvantage of FID is its failure to detect inorganic compounds. However, the advantages prevail for organic systems due to its linear response and high sensitivity of about 10^{-7}. The detector Linearity was verified using different mixtures of ethane in helium by FID connected to a HP 9800 GC. These mixtures were prepared by metering the flows of helium and ethane. According to the results provided in Fig. 4.3, FID passes sensitivity and calibration tests even at very low concentrations of ethane.

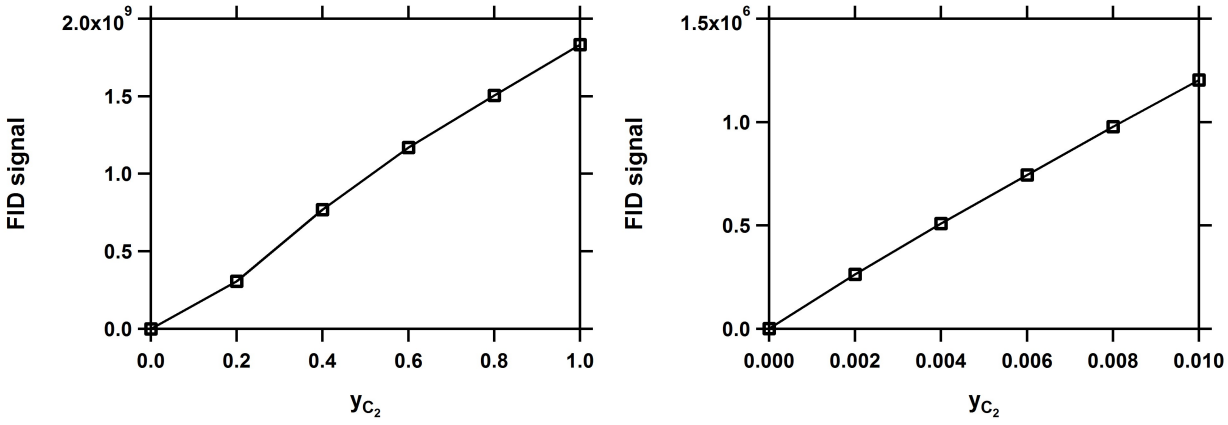

(a) (b)

Figure 4.3: Flame ionization detector calibration curves at (a) high and (b) low concentrations.

Thermal Conductivity Detector

The Thermal conductivity detector (TCD) measures the thermal conductivity of the gas and compares it with a reference gas (i.e. He or H_2). The most significant advantage of this equipment is its ability to detect both the organic and inorganic compounds. Pre-

liminary tests on TCD sensitivity and linearity, are shown in Fig. 4.4 indicates that The TCD signal was linear for low concentrations of ethane in He (lower than 2%). However, at higher concentrations, the TCD signal saturates at compositions higher that 2%. Although the test gas in the ZLC experiments were dilute enough to be in TCD linearity range, the signal itself was not as strong as FID at very low concentrations.

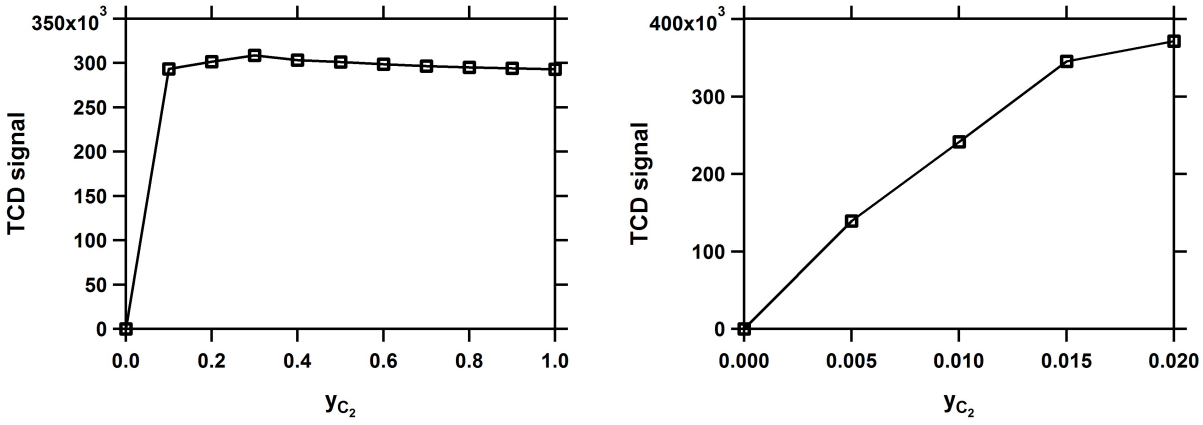

(a) (b)

Figure 4.4: Thermal conductivity detector calibration curves at (a) high and (b) low concentrations.

Mass Spectrometer

Mass spectrometry is a well-proven analytical technique to measure the gas concentrations. The major advantage of mass spectrometry is its application in multi-component systems. In this instrument, the inlet gas is exposed to an electron emission which results in ion generation. The analyzer separates the ions by electric or magnetic fields in which each mass to ion ratio produces a specific ion current [53]. The ion current is related to the partial pressure of the specific component by:

$$I = \bar{S}P \tag{4.1}$$

where ($\bar{S}$) is the effective sensitivity of the system which is function of gas species and the analyzer properties. This linear relationship between the ion current and the pressure can

only be applied to a certain pressure range. The linearity check of the mass spectrometer should be performed in the pressure range of interest. Different mixtures of ethane in helium were tested using the blank ZLC set-up. The results are described in Fig. 4.5. No linear relationship between the component ion current and the corresponding pressure was observed. As illustrated in Fig. 4.5b, MS showed limited repeatability.

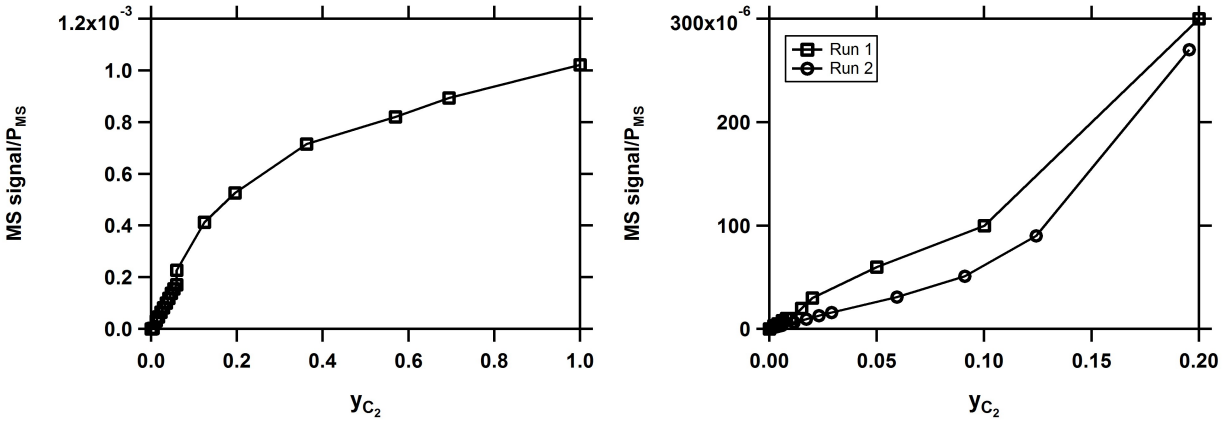

(a) (b)

Figure 4.5: Mass spectrometer calibration curves for (a) high and (b) low concentrations.

From the above experiments, it is clear that among the detectors studied, the FID suited the needs of the current study. Thus, it was chosen for further experiments.

4.4 Data analysis

The digital detector signal was normalized using:

$$\frac{C}{C_0} = \frac{S}{S_{\max}} \tag{4.2}$$

to obtain ethane composition in the effluent stream. In this equation, maximum signal ($S_{\max}$) is the average signal before switching, i.e. when the test gas was still flowing through the system (highest concentration, C_0).

In addition, the detector has few seconds as dead volume and response time. Several blank runs were completed at different flow rates to measure the detector response time. In these experiments, 1/8" tubing was added to increase the system dead volume, and to make the first few seconds more sensible. Figure 4.6 shows the results at 5, 10 and 20 sccm and the repetitions, note that in these experiments t=0 represent the time at which the gas was switched from test to purge gas. The effects of pressure fluctuations on the detector response results were observed over the first few seconds after switching. In order to minimize these fluctuations, pressure in the purge line were set using the needle valves prior to the switching time.

Blank runs at a specific flow rate must overlap. According to Fig. 4.6, the detector response time was understood to be the main cause of variations in the results. This response time is dependent on different factors such as environment effects and the detector conditions. Therefore, it varies from experiment to experiment. Different values as detector response time were assumed (t_1, t_2, t_3) and analyzed as shown in Fig. 4.7. These different values represent the local minimum and maximums from t=0 to when desorption begins (signal drops).

In order to get the comparable results for each flow rate, desorption curves were shifted on the time scale to match the local maximum or minimum points. After off-setting all the

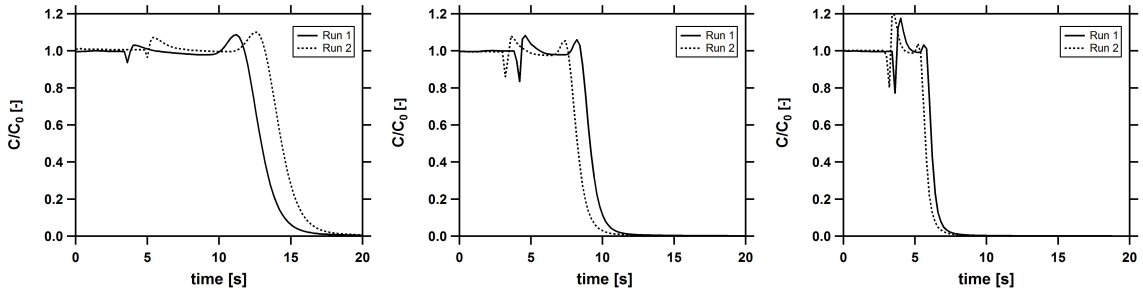

(a) 5 sccm (b) 10 sccm (c) 20 sccm

Figure 4.6: Blank runs with extra volume at different flow rates (5, 10, 20 sccm). The time t=0 denotes the moment when the purge gas is switched from the test gas.

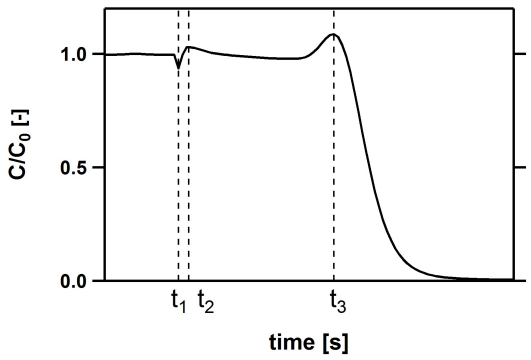

Figure 4.7: Schematic demonstration of studied correction times (t_1, t_2, t_3).

responses using t_1 (the local minimum point), different tests of each flow rate overlapped. Results after correction are illustrated in Fig. 4.8. The same steps were replicated for t_2 and t_3. However, the off-setted signals did not overlap. Comparing Figs. 4.6 and 4.8 shows that the detector response time varies from one experiment to another. This value, t_1, would need to be off-setted from all the ZLC desorption responses.

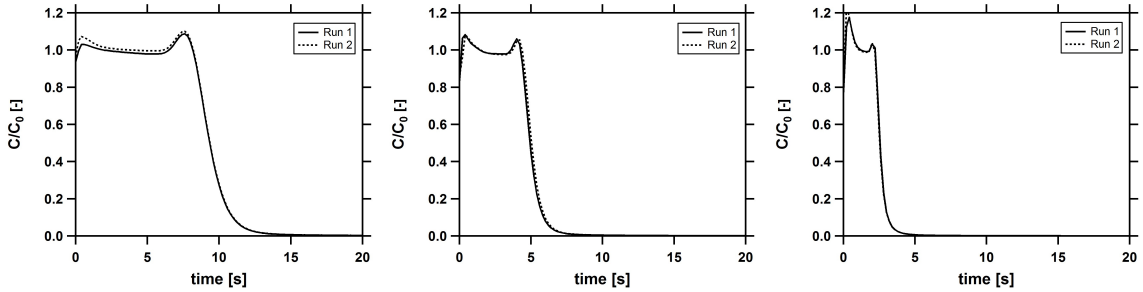

(a) 5 sccm (b) 10 sccm (c) 20 sccm

Figure 4.8: Blank runs with extra volume at different flow rates (5, 10, 20 sccm) after correction.

4.5 Dead volume measurement

As discussed earlier, dead volume, V_g is an important factor in experiments especially for weakly adsorbed systems, and for experiments using small amounts of adsorbent. The dead volume in ZLC systems is defined as all the tubing and the ZLC cell between the

switching valve and the detector. In order to measure the system dead volume, blank tests have to be carried out using an empty ZLC column. The area under desorption response curve in Ft plot corresponds to the system dead volume. This value should be subtracted from all the ZLC responses to avoid errors in analysis. Figure 4.9 shows the ZLC blank experiments performed at different flow rates (5-50 sccm). In these experiments, 1% ethane in helium is the test gas, and pure He is used as the purge gas. The total measured dead volume of the ZLC set-up is $\sim$ 0.5 cc. It is also observed that the time required for $\frac{C}{C_0}$ to reach a value of 0.0001 at flow rate of 50 sccm is $\sim$ 20 seconds.

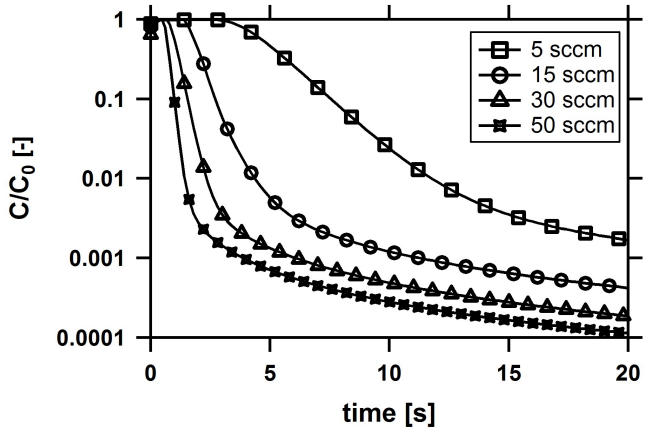

Figure 4.9: Blank ZLC responses at different flow rates.

4.6 Isotherm measurement

The adsorption isotherms were measured using high pressure adsorption analyzer (HPVA-100) from VIT scientific instruments. This volumetric system contained a dosing cell and a sample cell with known volumes (V_{dose} and V_{sample} respectively). There are a number of pressure transducers and sensitive thermocouples installed in each of these cells that monitor pressure and temperature data. First, an adsorbent sample with a known mass was loaded in the sample cell. This cell was then evacuated and out-gassed. Meanwhile, the dosing cell filled with the test gas. A known volume of the test gas was transferred from the dosing cell to the sample cell through the tubing and the valves. System dead

volume (V_{dead}) was taken into account, and the gas densities were calculated using the system conditions in the cells and the dead volume. The experiment measured the excess adsorption which can be calculated from the mass balance around the whole system described by:

$$n_{\text{ads}} = \frac{(\rho_{\text{dose,a}} - \rho_{\text{dose,b}})V_{\text{dose}}}{m_{\text{ads}}} - \frac{(\rho_{\text{sample,a}} - \rho_{\text{sample,b}})(V_{\text{sample}} - V_{\text{solid}})}{m_{\text{ads}}}$$

$$- \frac{(\rho_{\text{dead,a}} - \rho_{\text{dead,b}})V_{\text{dead}}}{m_{\text{ads}}} \tag{4.3}$$

where a and b are the initial and the final conditions of the experiment, ρ_{dose}, ρ_{sample}, and ρ_{dead} are the densities of gas in each section calculated using the pressure and temperature of the system, V_{dose} and V_{sample} are the volumes of the two cells, m_{ads} is the adsorbent mass. Results are shown and discussed in Chapter 5.

4.7 Solid characterization

Prior to the analysis of the ZLC curves, the solid has to be characterized. For this purpose, three experiments, namely, thermo-gravimetry, mercury porosimetry, and nitrogen adsorption were performed.

4.7.1 Thermo-gravimetric analysis (TGA)

In thermo-gravimetric analysis, the sample was activated to the regeneration temperature, and its weight was monitored. First, 2-GA sample was prepared (around 70 mg), and placed on the instrument tray. The unit was programmed to follow a defined procedure: measure weight of the tray; increase system temperature to 200°C, maintain temperature at 200°C for 15 minutes till no deviation in weight; cool down to 30°C. The monitored weight of 2-GA activated carbon sample and the recorded temperatures are shown in Fig. 4.10. The result demonstrates that the activated carbon sample used in this study loses approximately 3% of its weight after regeneration.

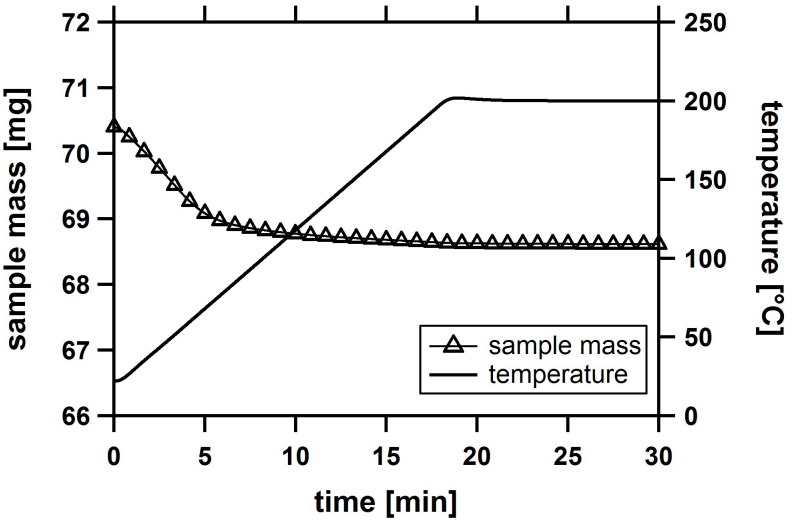

Figure 4.10: Thermo-gravimetric analysis result for 2-GA activated carbon with sample weight of 70.409 mg.

4.7.2 Mercury porosimetry

Porosimetry is the term used for physical property measurements such as pore size distribution, solid density, porosity, and tortuosity. Mercury porosimetry is one of the techniques widely used for these measurements. This method is based on non-wetting property of mercury and its high surface tension [18]. Because of these characteristics, mercury needs an external force (pressure) to penetrate small pores. The required pressure is inversely proportional to the inner width of the pore. The relationship between the pressure and the pore size is given by Washburn equation (Eq. (4.4)) which can be derived by a force balance:

$$\Delta P = \frac{2\gamma \cos\theta}{r_{\mathrm{p}}} \tag{4.4}$$

where γ is mercury surface tension (0.485 N m^{-1}); θ is contact angle of mercury and the surface, which is approximately 140°. Using this equation, if the pressure applied to mercury is known, the minimum diameter of pores in which mercury enters to can be calculated.

During the experiment, pore size corresponding to each pressure point is calculated by the software, and the mercury penetrated volume is also measured [54]. Mercury porosimetry can reach pores between 500 to 0.005 μm which are categorized as macropores and mesopores. The apparatus has two different ports; one for low and the other for high pressure measurements. Low pressure range is typically around 4 to 300 kPa, and high pressure test is performed for pressures above this range. The difference in the two operations is the environment of the experiment. The low pressure test was open to atmosphere. While, hydraulic oil is used for high pressure operation. When mercury intrusion is completed (both low and high pressure), mercury extrusion starts by reducing the applied pressure. Extrusion shows sample hysteresis. For this reason extrusion results are usually different from the intrusion result because there is no driving force to take mercury out of the pores.

Mercury porosimetry measurements in this study were perfomed on Quantachrome Poremaster. Two different samples were prepared (0.5697 and 0.5875 g) and tested on different days. Each sample was placed in the sample cell (penetrometer), and low pressure operation started. After low pressure measurement, cell was transferred into the hydraulic oil for high pressure operation. During the experiments, applied pressure and the measured mercury volume were monitored. Figure 4.11 illustrates the intrusion curves for both samples. In order to get a better picture, the calculated pore size distribution is shown in Fig. 4.12. The average pore size is calculated using the pore size distribution data. Sample porosity and tortuosity parameters measured by this technique are summarized in Table 4.1. The porosity of the sample was lower than the expected values reported by literature [15]. According to the mercury intrusion plot, the maximum intruded volume was approximately 0.25 $cc.g^{-1}$, and the particle density of the sample was around 0.75 $cc.g^{-1}$. As a result, the estimated porosity of the 2-GA activated carbon was 0.33. It is worthwhile to mention that these values are measured and calculated for macropores and mesopores, however, activated carbon is well-known for its developed micropore structure. For this reason, BET analysis was performed on the 2-GA activated carbon sample which is explained in detail in the next section. From the mercury porosimetry

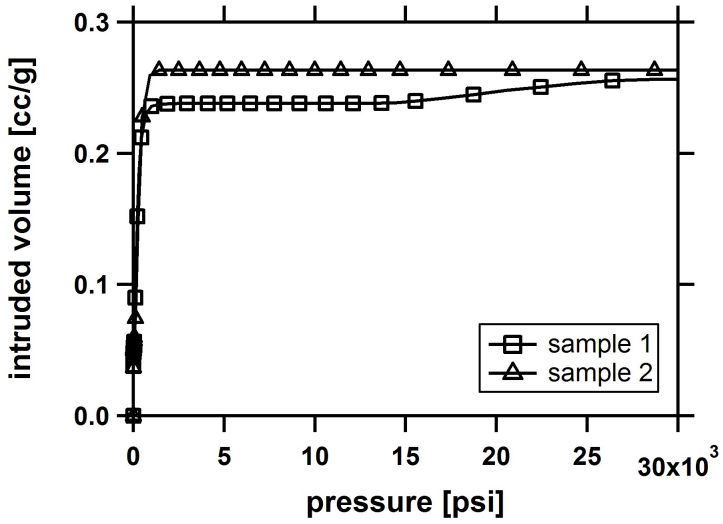

Figure 4.11: Mercury intrusion curves for 2-GA activated carbon samples.

experiments, it is evident that there are variations in the pore size distribution from one sample to the other. These sample variations are not uncommon in activated carbons, and can be formed during the manufacturing process.

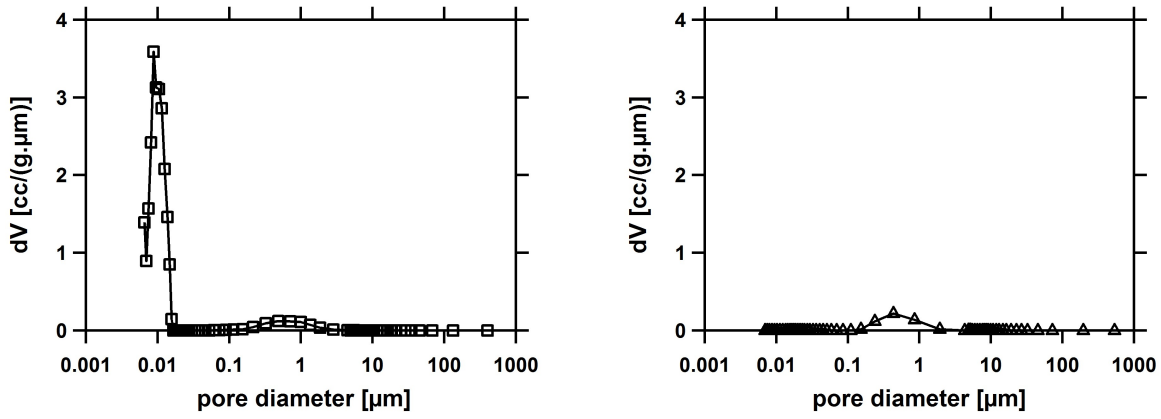

(a) sample 1

(b) sample 2

Figure 4.12: Pore sized distribution of 2-GA activated carbon from mercury porosimetry experiments.

Table 4.1: Properties of 2-GA activated carbon obtained from mercury porosimetry measurements

Sample No	Average pore diameter $[\mu m]$	Porosity [-]	Tortuosity [-]
1	1.4	0.119	2.057
2	1.2	0.119	2.055

4.7.3 Nitrogen adsorption measurement

Gas adsorption is a remarkable technique to study physical characteristics of porous materials such as surface area and pore size distribution. This method gives a better understanding of microporous structure inside the solid particles [55]. According to IUPAC classification, pores with width smaller than 2 nm are called micropores. Different types of apparatus are used for this purpose which are divided into two groups; (a) manometric measurement (b) uptake rate measurement [17].

In this work, manometric measurements were performed using Quantachrome Autosorb to characterize 2-GA activated carbon particles. These measurements were completed under isothermal condition. A known volume of gas was exposed to a cell containing the adsorbent. After sufficient time the system reached the equilibrium and the pressure dropped due to adsorption. The adsorbed amount is defined as the difference between the exposed volume and the gas remaining in the chamber which can be calculated by system pressure. This procedure provides adsorption isotherm for the gas used in the experiment at the defined temperature. Experimental data was processed through an available software to determine the surface area, micropore volume and pore size distribution.

Brunauer, Emmerr, and Teller established a theory (1938) to analyze surface area of nanoporous materials [56]. BET theory is a simplified isotherm model that can be applied for a specific range of pressure. In this analysis, N_2 at its boiling point (77 K) is traditionally used due to its availability. Argon and Krypton are the alternative

adsorbates for this purpose. In order to determine BET surface area, measured adsorption isotherm should be transformed to BET Plot. This plot is linear within the $\frac{P}{P_0}$ range of 0.05 to 0.3, expressed by BET equation:

$$\frac{1}{V_{\mathrm{a}}(\frac{P_0}{P}-1)} = \frac{C-1}{V_{\mathrm{m}}C}\frac{P}{P_0} + \frac{1}{V_{\mathrm{m}}C} \tag{4.5}$$

$\frac{P}{P_0}$ is the relative pressure (at 77 K), V_{a} is the gas volume adsorbed at STP conditions (273.15 K and 1 atm), V_{m} is the gas volume adsorbed at STP to build the adsorbed monolayer on the solid surface, and C is the constant related to interaction between gas and liquid. By plotting $\frac{1}{V_{\mathrm{a}}(\frac{P_0}{P}-1)}$ against $\frac{P}{P_0}$, V_{m} can be calculated from the slope and the intercept; this value is directly related to the sample surface area (S_{BET}) by equation below:

$$S_{\mathrm{BET}} = \frac{V_{\mathrm{m}}Na}{22400m_{\mathrm{ads}}} \tag{4.6}$$

In this equation N is Avogadro constant ($6.02\times\ 10^{23}$), a is cross sectional area which is 0.162 nm^2 for N_2, m_{ads} is adsorbent mass. Two samples of 2-GA activated carbon were prepared for gas adsorption analysis (0.0475 and 0.0408 g). BET analysis for the samples are shown in Fig. 4.13. Calculated BET surface area (S_{BET}) for the samples are 1036

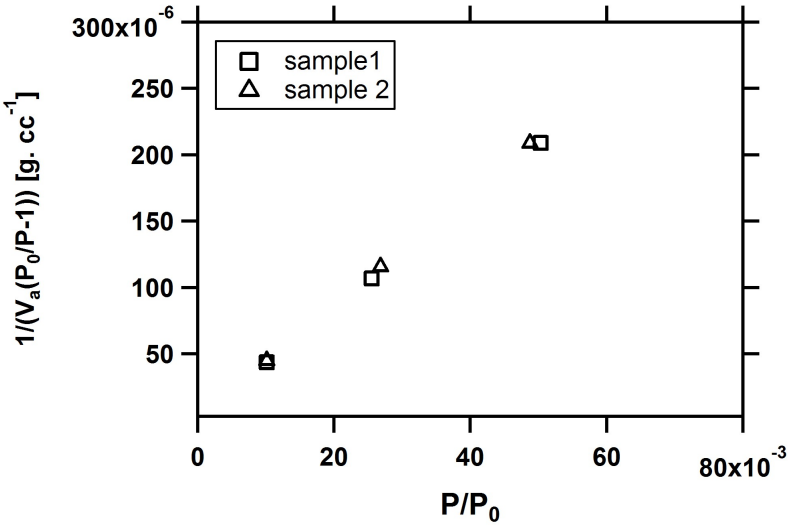

Figure 4.13: BET plot of 2-GA activated carbon samples from N_2 adsorption experiments.

$[\frac{m^2}{g}]$ and 1012 $[\frac{m^2}{g}]$ respectively.

If adsorbed film thickness is assumed to be uniform at each equilibrium stage, the thickness can be obtained by adsorption isotherm. There are several equations to calculate film thickness as a function of relative pressure. With no micropores in sample, plotting adsorbed volume against thickness results a straight line which crosses the origin. However, in the presence of micropores, the straight line shows a positive intercept (i) that is equivalent to micropore volume (see Eq. 4.7) [57].

$$V_{\text{micro}}[\frac{cc}{g}] = 0.001547i \tag{4.7}$$

V-t plots for 2-GA activated carbon samples are shown in Fig. 4.14. Micropore volumes calculated by intercepts for the first and the second samples are 0.35 and 0.34 $\frac{cc}{g}$ respectively.

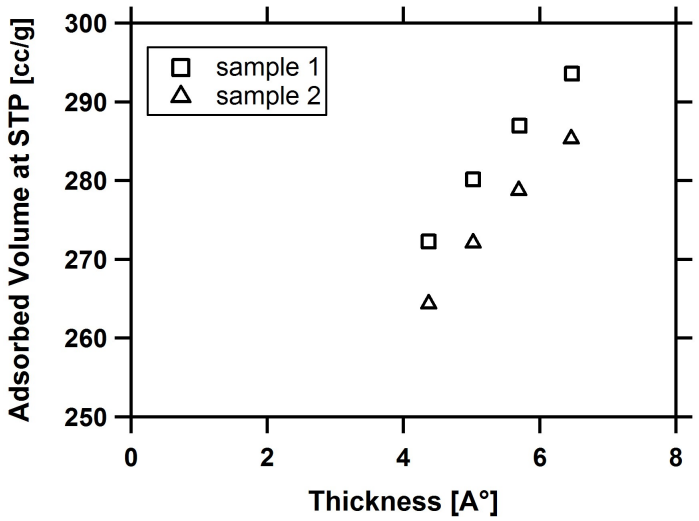

Figure 4.14: V-t plot of 2-GA activated carbon samples obtained from N_2 adsorption experiments.

The software, also, provides pore size distribution using Density Functional Theory (DFT) [55]. This method is based on statistical mechanics, in which adsorbate is considered as an inhomogeneous fluid; its density profile changes across the pore. Different

pores are assumed to be identical in shape. Pore size distribution results obtained from N_2 adsorption experiments for both samples are illustrated in Fig. 4.15. The average pore width calculated for these two samples are 0.0018 and 0.0020 μm respectively.

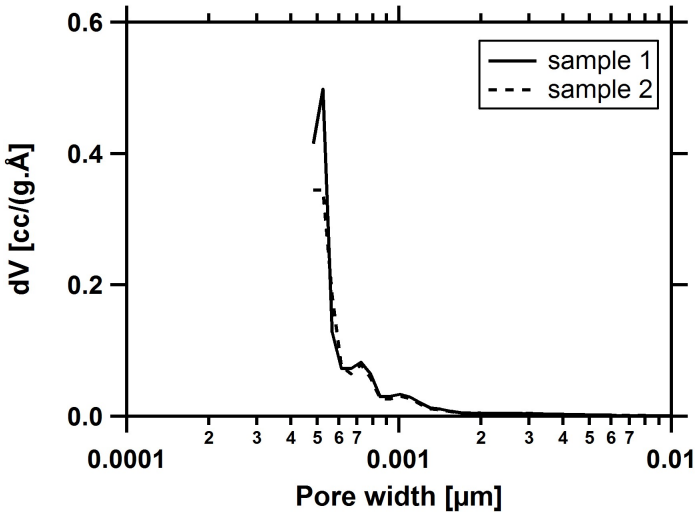

Figure 4.15: Pore size distribution of 2-GA activated carbon samples from N_2 adsorption measurement.

4.7.4 Conclusion

In order to characterize adsorbent used in this study, mercury porosimetry and N_2 adsorption measurements were carried out on the 2-GA activated carbon sample. Mercury porosimetry is a well-known technique for characterization of macro- mesopores; while, N_2 analyzes micropores of the porous solid. Combining of the results obtained from the two measurement techniques provides an insight to explain the pore structure of the sample under study. Figure 4.16 shows the combined results. According to this figure, the activated carbon sample exhibits bimodal pore distribution. Both macro- and micropores are present in the pore structure, and the micropores fraction is more significant.

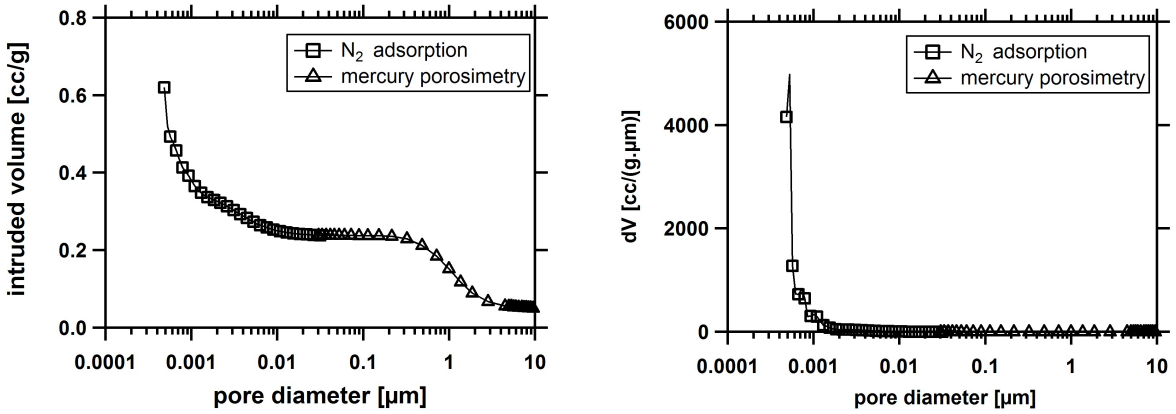

(a) (b)

Figure 4.16: Pore size distribution of 2-GA activated carbon obtained from mercury porosimetry and N_2 adsorption.

Chapter 5

Results and Discussion

The details of diffusion mechanisms, measurement techniques, and theory of zero length column; its mathematical model, and experimental set-up have been discussed in the preceding chapters. System characterization measurements such as dead volume determination and solid physical property measurements have been presented too. This chapter is reserved for the experimental results of volumetric measurements and zero length column technique. These experiments provide further analysis on determination of diffusion mechanism of dilute ethane in 2-GA activated carbon.

5.1 Isotherm measurements

Adsorption equilibrium is described by adsorption isotherms; a plot of the adsorbed phase concentration as a function of the concentration of adsorbate in the gas phase or its partial pressure. Physical adsorption isotherms are divided into different categories. Microporous materials have the pore sizes close to the gas molecular dimensions. They are usually described by type I isotherm with a monotonic curvature and finite saturation capacity as shown in Fig. 5.1 [12]. Isotherms give useful information about the system under study such as the capacity and the strength of the adsorbent for a specific component or mixture. At very low gas concentrations, the relationship between the two phases is linear and is expressed in:

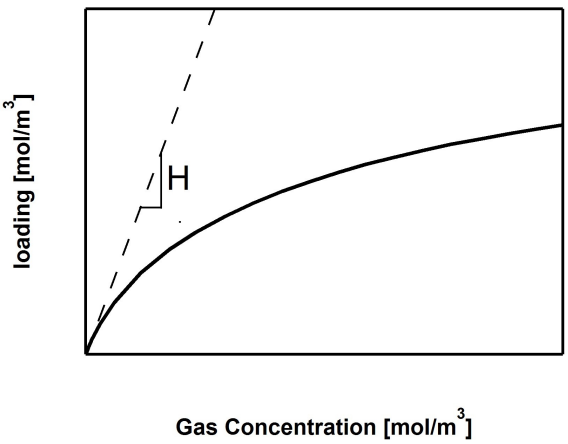

Figure 5.1: Qualitative description of type I isotherm and Henry's law constant.

$$q = HC \tag{5.1}$$

where q is the concentration of the adsorbed phase and C is the concentration of adsorbate in the gas phase. This condition is known as Henry's Law and the slope is called Henry's Law constant (see Fig. 5.1). At higher concentrations, isotherms deviate from the linear form and become curved [38]. There are different mathematical models that predict the behavior of adsorption isotherms by a number of parameters. The Langmuir isotherm is perhaps the simplest model which is commonly used to describe adsorption equilibrium as shown below:

$$q = \frac{q_s bC}{1 + bC} \tag{5.2}$$

In the above equation, q_s, b, and C are saturation capacity, affinity parameter, and fluid phase concentration, respectively. The affinity parameter (b) is described by

$$b = b_0 exp(-\frac{\Delta U}{\mathrm{R_g} T}) \tag{5.3}$$

where b_0 is the pre-exponential factor, ΔU is the the internal energy of adsorption, T is temperature, and $\mathrm{R_g}$ is the ideal gas constant. In this model, it is assumed that adsorption on the surface is a monolayer, each site can accommodate only one adsorbed molecule, different sites are energetically homogeneous, and there is no interaction between the

neighbouring adsorbed molecules [12]. Moreover, Henry's Law constant is defined as $H = q_s b_i$ at each temperature. Langmuir model fails to describe adsorption equilibrium in many systems where the adsorbent is structurally heterogeneous [12].

Dual-site Langmuir is a modification of the single-site model. In this modified model, it is assumed that two energetically distinct sites are present in the solid structure, and each site shows Langmuirian equilibrium behavior [12]. There are three fitting parameters for each site, q_{sb}, b_0, ΔU_b, and q_{sd}, d_0, ΔU_d which are defined in the same manner as described above. The dual-site Langmuir has the following form:

$$q = \frac{q_{s\mathrm{b}} bC}{1 + bC} + \frac{q_{s\mathrm{d}} dC}{1 + dC} \tag{5.4}$$

$$b = b_0 exp(-\frac{\Delta U_{\mathrm{b}}}{\mathrm{R_g} T}) \tag{5.5}$$

$$d = d_0 exp(-\frac{\Delta U_{\mathrm{d}}}{\mathrm{R_g} T}) \tag{5.6}$$

5.1.1 Volumetric measurement

Isotherms at different temperatures (30, 50, and 70°C) for the system under study were measured using volumetric technique. In these experiments, activated carbon particles were loaded in the sample cell, and C_2 was transferred to the cell at known partial pressures. The adsorbed amount for each pressure step was calculated by a mass balance. In the present study, the experimental data for low pressures were modelled using dual-site Langmuir isotherm. In order to achieve this, non-linear regression of experimental data for all the three temperatures was performed and the six parameters of the dual-site

Table 5.1: Dual-site Langmuir parameters for ethane on 2-GA activated carbon

$q_{s\mathrm{b}}$ [mol/kg]	$q_{s\mathrm{d}}$ [mol/kg]	$\mathrm{b_0}$ [$\mathrm{m^3}$/mol]	$\mathrm{d_0}$ [$\mathrm{m^3}$/mol]	-ΔU_{b} [kJ/mol]	-ΔU_{d} [kJ/mol]
1.58	3.8	4.04×10^{-4}	7.6×10^{-7}	19.025	27.813

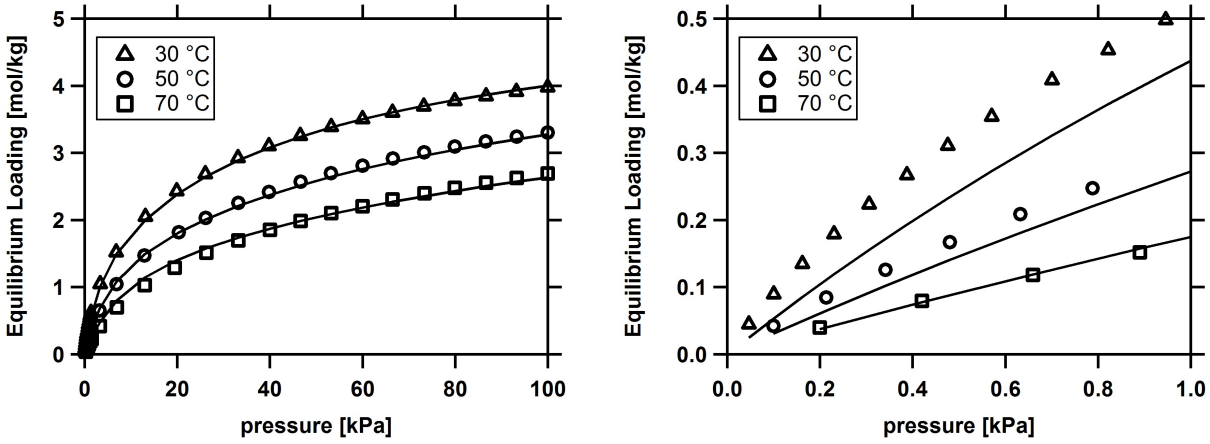

(a) (b)

Figure 5.2: Adsorption isotherms of ethane on 2-GA activated carbon up to (a) 100 kPa and (b) 1 kPa markers are experimental points and lines are fitted using dual-site Langmuir model.

Langmuir model were fitted. The fitted parameters are summarized in Table 5.1. Adsorption isotherms and the comparison between the experimental results and the fitted model are illustrated in Fig. 5.2a. According to this figure, isotherms show non-linear behavior close to the atmospheric pressure. Ethane Isotherms for low concentrations (below partial pressure of 1 kPa) are also shown in Fig. 5.2b where deviation from the Henry's Law can be seen even at this pressure range.

5.1.2 Equilibrium measurement using ZLC

As discussed in Chapter 4, ZLC experiments can be performed either under equilibrium controlled conditions at low flow rates or non-equilibrium conditions where kinetics play the leading role. Under equilibrium conditions, the plot of normalized concentration ($\frac{C}{C_0}$)vs. Ft (volumetric flow $\times$ time) at different flow rates overlap, and equilibrium data can be obtained from the ZLC responses [38]. This feature was used for rapid adsorbent screening in carbon capture by Hu et al. [35]. On the other hand, in a non-equilibrium system, there is a point when desorption curves at different flow rates cross in the above-mentioned plot, and they diverge by increasing the flow rate [42]. ZLC experiments at

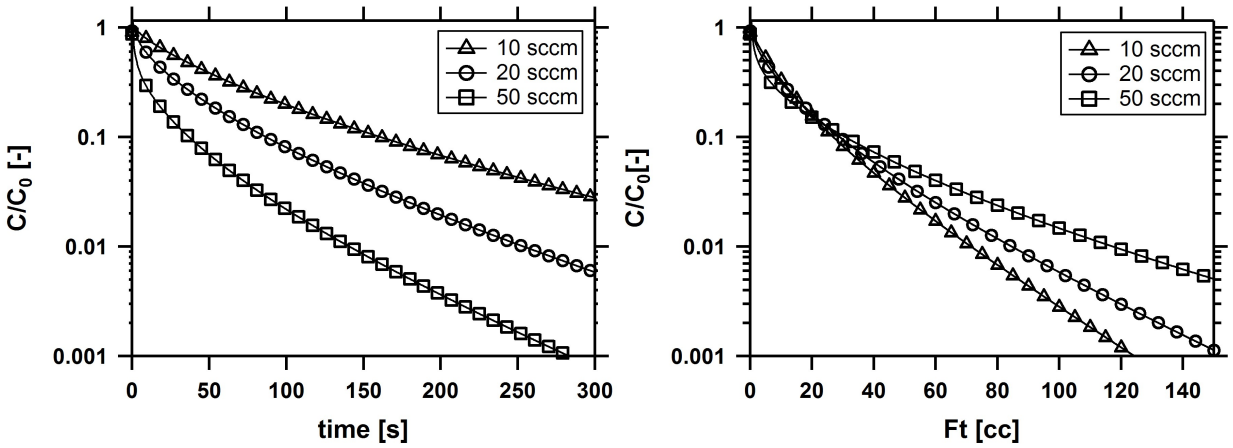

(a) (b)

Figure 5.3: Experimental ZLC response curves of 2-GA activated carbon at 0.01 atm of ethane at 30°C.

different flow rates over a sample of 2-GA activated carbon (10.1 mg) were carried out at 30°C. Figures 5.3a and 5.3b show desorption curves and the Ft plot at flow rates of 10, 20, and 50 sccm. It is clear from Fig. 5.3a that as the flow rate increases, lower desorption times are obtained. Ft plot (Fig. 5.3b) also indicates that system is kinetically controlled, i.e. the cross points of different flow rates, and the divergence of the curves .

According to the ZLC mathematical model, both equilibrium and kinetics data can be obtained from desorption curves in such systems. Figure 5.4 illustrates the comparison between the predicted equilibrium behavior calculated by the ZLC experiments at flow rates of 10, 20, and 50 sccm and the isotherm measured by the volumetric method. There is an apparent discrepancy between the behaviors of the two data sets. The measured Henry's law constants by the ZLC experiments are lower than the predicted values by volumetric technique, and it decreases by increasing the flow rate. It is recommended to obtain equilibrium data by performing ZLC experiments at low flow rates where equilibrium is dominant [39]. ALICAT flow controllers used in the ZLC set-up, fluctuate at flow rates below 10 sccm, therefore lower flow rates were not accessible using the current ZLC set-up. This behavior might be resulted by a number of reasons. It might be caused by the uncertainties in the first seconds of the experiment and the way the detector response

time was corrected. It may be concluded that the particle under study may not be a perfect representative of the entire particles, and considerable heterogeneity is expected among the particles. Also, small quantities of water may be present in the gas cylinders which reduced the capacity of the sample. Therefore, fitted parameters of volumetric measurements are used for equilibrium data in the present study.

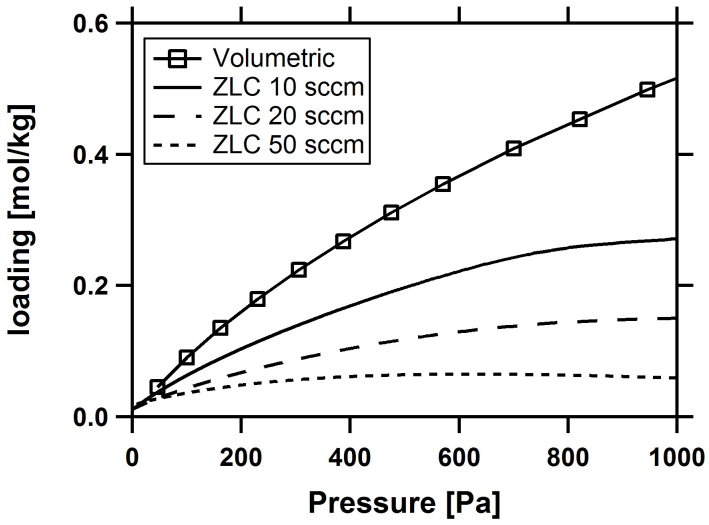

Figure 5.4: Comparison of ethane isotherms by ZLC experiment at 10, 20, and 50 sccm and the volumetric measurement (T=30°C).

5.2 Diffusion measurements

In ZLC experiments, external heat and mass transfer resistances are eliminated due to high flow rates of purge gas, small amount of adsorbent, and low adsorbate concentrations. Therefore, mass transfer is only controlled by gas diffusion out of adsorbent particles [39]. According to Chapter 2, there are several different diffusion mechanisms that can control the kinetics. Figure 5.5 shows the experimental checks for each diffusion mechanism. In the current study, each mechanism was tested independently. The Zero length column experiments of dilute ethane (1% in helium as the inert carrier gas) on 2-GA activated carbon particles were performed at different flow rates, particle sizes, temperatures, and purge gas types to determine the diffusion parameters. The results are discussed in this section.

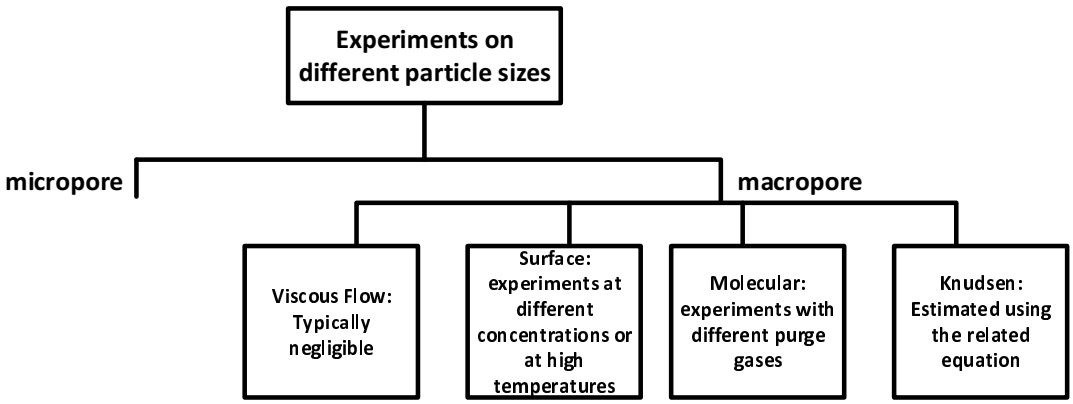

Figure 5.5: Summary of different diffusion mechanism and their experimental checks.

5.2.1 Experiments with different particle sizes

In order to determine the controlling diffusion mechanism for the system under study, experiments using different particle sizes were first performed. According to the ZLC mathematical model, desorption curves in a semi-logarithmic plot of normalized concentration versus time have a linear asymptote at sufficiently long times [14]. The effective diffusional time constant of the system can be calculated using the slope of the long time asymptote; the relationship between the effective diffusional time constant ($\frac{D_e}{R^2}$) and the slope of the asymptote is linear. If mass transfer is controlled by diffusion in the micropores the slope of the long time asymptote will not depend on the particle radius (R), but the crystal size of the adsorbent. On the other hand, if the controlling mechanism is diffusion of the gas in the macropores this slope will be inversely proportional to the square of the particle radius [43].

According to Mayfield and Do [15], kinetics of ethane adsorption in activated carbon is controlled by gas diffusion in both micropores and macropores, due to the bidisperesed pore size distribution. Micropore diffusion contribution can be investigated by ZLC experiments on different particle sizes, as mentioned above. the ZLC experiments were carried out on one activated carbon particle (A, 7.5 mg) at two different temperatures. Activated carbons are well-known for their heterogeneous structure, due to their production proce-

dure. Therefore, the sample was crushed, and the same experiments were performed on a crushed particle (B, 1.5 mg), in order to avoid heterogeneity in the system. The ZLC long time approach was applied at very low concentrations. At this region, the diffusion is controlled by those gas molecules which are passing through the longest path to come out of the particle, which corresponds to the largest dimension of the particle [43]. The largest diameter of the particles, were estimated to be 3.74 and 2.1 for particle A and B, respectively, and used for all the diffusion calculations.

Figure 5.6 shows the ZLC desorption curves for the uncrushed and the crushed samples. It is clear that the desorption rate depends strongly on the particle size which is an evidence of macropore diffusion control. It should be noted that the mass of the samples (uncrushed and crushed) used in the experiments are different, and this affects the adsorbed amounts, represented by area under the curves. For this reason, the experimental results are not compared in the same figure. The calculated and the measured values of diffusional time constants and particle diameters are summarized in Table 5.2. The diffusional time constants obtained from the desorption curves indicate that the ratios of 3.55 and 3.38 at 30°C and 50°, respectively, are comparable to the ratio of the square of the particle diameters which is 3.2. This is the experimental confirmation that macropore diffusion controls the mass transfer of ethane in the activated carbon particle, and micropore resistance can be neglected at these experimental conditions.

Table 5.2: Summary of time constants for ZLC desorption curves from different particle sizes of activated carbon

Sample	Slope at 30°C [1/s]	Slope at 50°C [1/s]	Diameter [mm]
A	-0.018	-0.037	3.74
B	-0.064	-0.125	2.1

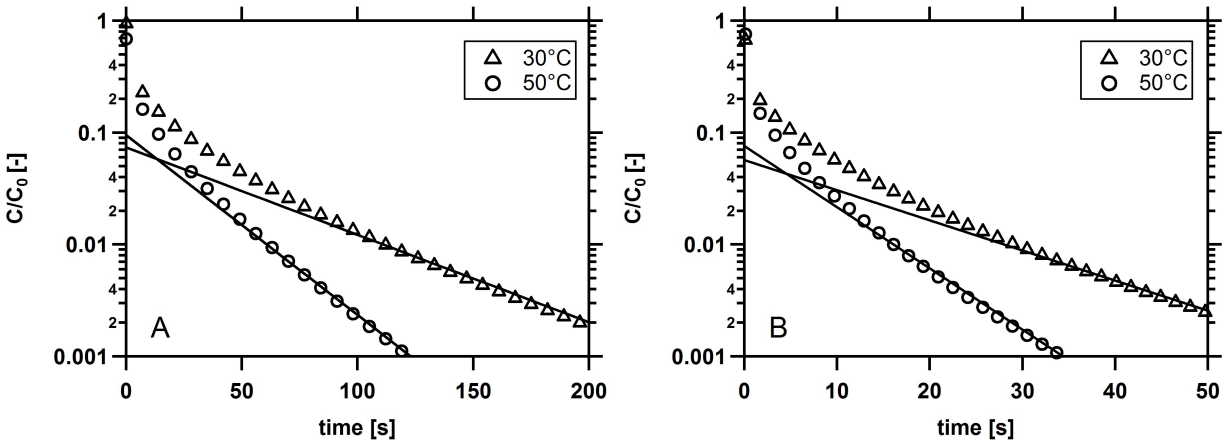

Figure 5.6: Experimental ZLC desorption curves for uncrushed (A) and crushed (B) samples at $T = 30°$C and 50°, 50 sccm.

5.2.2 Estimation of macropore diffusivity

As discussed in Chapter 2, viscous flow diffusion mechanism takes place when ΔP across the pores is significant. However, in systems with few adsorbent particles such as the system under study in this project, ΔP is negligible. Thus, the contribution of this mechanism is ignored. As mentioned earlier, surface diffusion is strongly dependent on the concentration of the adsorbed species or adsorbed layer thickness. As the adsorbed phase concentration increases, surface diffusion contribution increases as well. In some studies on activated carbons, it is reported that at high concentrations, the contribution of surface flux in the macropore diffusion is as high as 50% [27]. However, the concentration dependence is only valid beyond the Henry's Law region [29]. In the present study, diffusion is calculated at very long times and below 0.01% ethane in the total concentration. This puts us at very low adsorbed phase concentrations where surface coverage is estimated to be $0.025q_{\mathrm{s}}$. This allows to eliminate the contribution of surface diffusion under the current operating conditions. Therefore, molecular and Knudsen seems to be the possible contributing mechanisms in the present system.

Experiments with different purge gases

In order to check the contribution of molecular diffusion, experiments on a sample of 2-GA activated carbon were performed using helium and nitrogen as the purge gas. Changing the purge gas is another test that verifies macropore diffusion controls the mass transfer [14]. In these experiments, nitrogen is assumed to be an inert gas. It is worth to note, Park et al. [58] reported that nitrogen does adsorb in activated carbon. However, its Henry's constant is much smaller than that of ethane. ZLC experiments using one particle with the mass of 3.7 mg at 20, 30, and 50 sccm flow rates were conducted using the two purge gases. The resulting desorption curves and the Ft plots are shown in Figs. 5.7 and 5.8 for helium and nitrogen, respectively. Similar behaviors can be observed for both purge gases. In the Ft plots, different flow rates cross each other, and they are diverging which confirms non-equilibrium conditions [42].

The direct comparison of the high flow rate (50 sccm) desorption curves obtained from helium and nitrogen are illustrated in Fig. 5.9. Helium and nitrogen have different interactions with ethane molecules, affecting the macropore diffusion in the system. It should be noted that the amount of ethane adsorbed is proportional to the area under the desorption curves. These values were comparable for helium and nitrogen. According to Fig. 5.9, it is clear that the behavior of the ZLC response curves are dependent on the nature of the

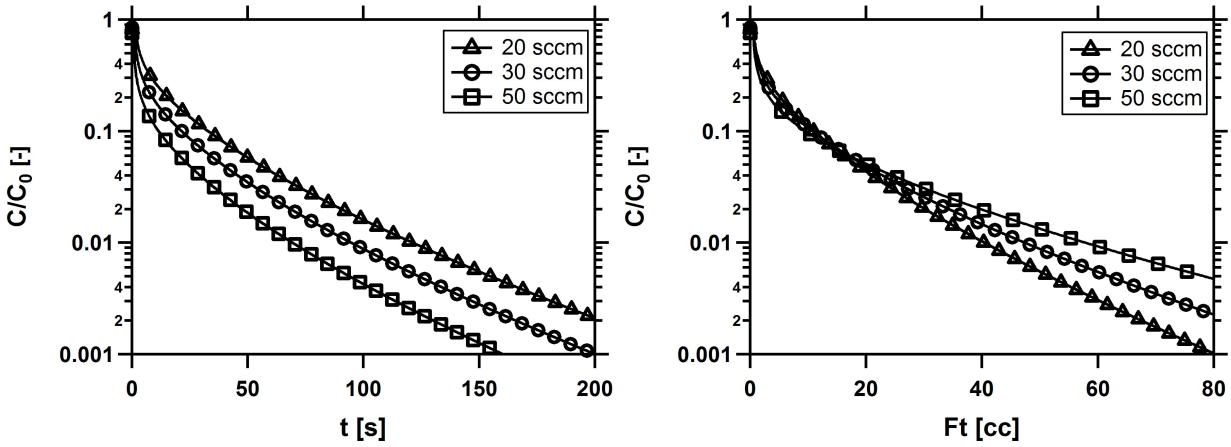

Figure 5.7: Experimental ZLC response curves of Activated carbon at 0.01 atm of ethane at 30°C, purging with helium.

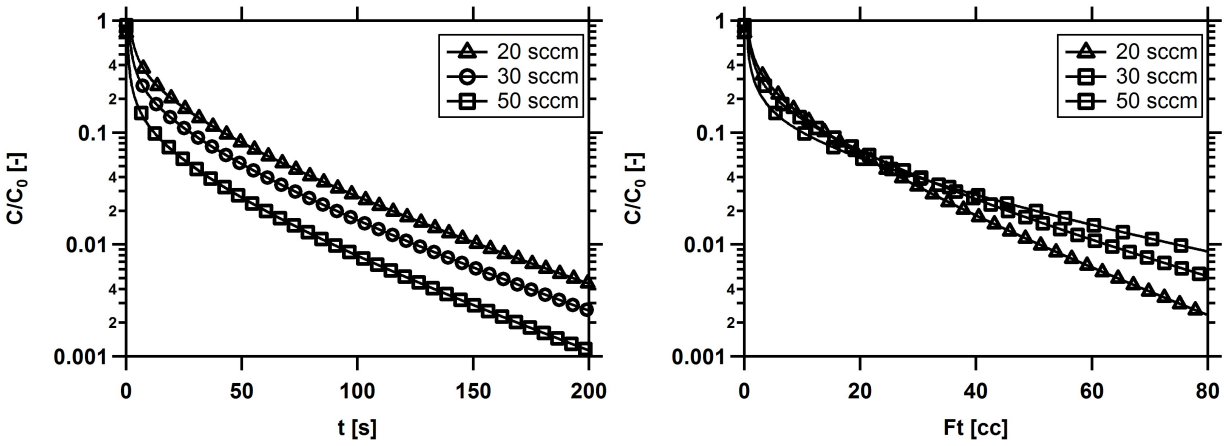

Figure 5.8: Experimental ZLC response curves of Activated carbon at 0.01 atm of ethane at 30°C, purging with nitrogen.

purge gas type. In other words, slopes of the long time asymptotes which are proportional to the effective diffusional time constants are different for helium and nitrogen. This provides the experimental confirmation that gas diffusion inside the macropores is an adding mechanism, and that molecular diffusion is contributing to the flux. The long time asymptote approach was used to estimate the diffusional time constants (D_e/R^2). The resulting parameters from the experiments and the calculated diffusivity ($Dtextsubscriptm, cal$), using Chapman-Enskog equation for each purge gas, are summarized in Table 5.3. There is a difference between the ratio of the slopes (1.33) and the ratio of the calculated molecular diffusivities (3.68). According to the calculated diffusional time constants, nitrogen dynamics was slower than that of helium. This can be explained by lower molecular diffusivity of ethane/nitrogen mixture compared with ethane/helium mixture. The same

Table 5.3: Parameters and calculated molecular diffusivity from helium and nitrogen ZLC desorption curves at 30°C and 50 sccm flow rate

Purge gas	slope [1/s]	D_e/R^2 [1/s]	intercept [-]	L [-]	$D_{m,\,cal}$ $[m^2/s]$
helium	-0.024	0.0027	0.044	46.4	5.9×10^{-05}
nitrogen	-0.018	0.0020	0.039	52.1	1.6×10^{-05}

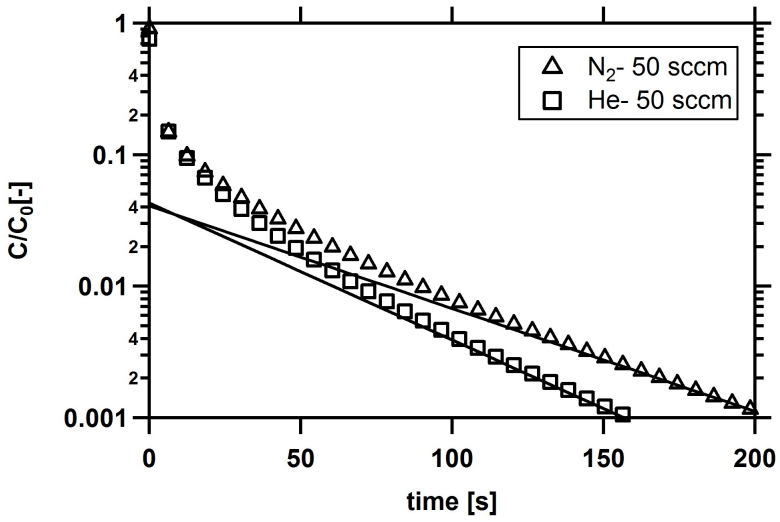

Figure 5.9: Comparison of experimental ZLC curves on activated carbon particle at 0.01 atm of ethane in two different purge gases (N_2 and He), at 30°C and 50 sccm.

behavior has also been reported by Do and Do [59], where mixture of ethane in helium and nitrogen (5% ethane) was used. The resulting dynamics for ethane/helium mixture was 4 times faster than that of ethane/nitrogen mixture. It should be mentioned that Knudsen diffusion was not taken to account in these calculations. According to these experiments, it is concluded that molecular diffusion has a major contribution to the total diffusivity in the system under study.

Experiments at different temperatures

Further analysis was performed by experiments on the same particle (3.7 mg) at different temperatures, 30, 50, and 70°C in order to determine macropore diffusivity of the system. Figure 5.10 illustrates the experimental results for desorption of 1% ethane over one particle of 2-GA activated carbon by purging helium at 50 sccm flow rate. A strong temperature dependence was observed in the desorption curves. The long time approach was applied to desorption curves, and ZLC parameters calculated as described in chapter 3. The resulting values are summarized in Table 5.4. Large L values confirmed that the experiments were performed under non-equilibrium conditions ($L > 10$) [14]. Increasing the system temperature, decreases the adsorbed amount of ethane on the adsorbent; also,

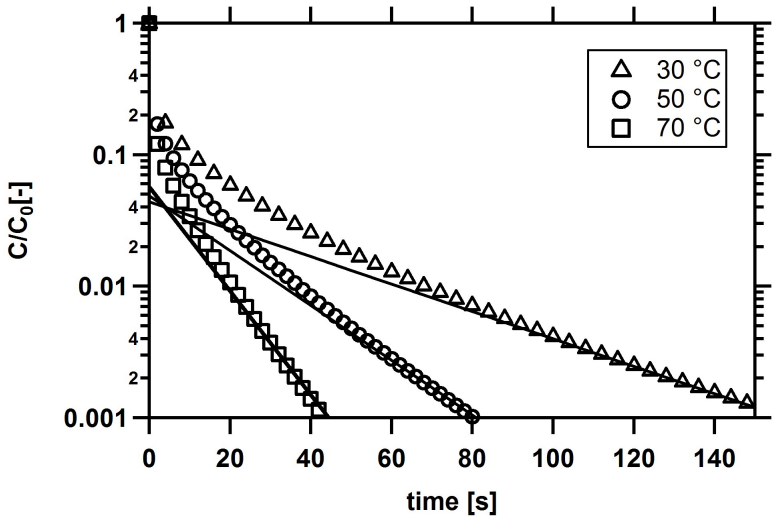

Figure 5.10: Comparison of experimental ZLC curves on activated carbon particle at 0.01 atm of ethane in two different purge gases (N_2 and He), 30°C and 50 sccm.

decreases the effective Henry's law constant (K). On the other hand, effective diffusional time constant (slope of the asymptote) and pore diffusivity increase.

According to Eq. (5.7), effective diffusivity (D_e) is related to the effective Henry's law constant (K), and pore diffusivity (D_{macro}), porosity (ϵ_p, void fraction) and tortuosity (τ) of the particle; described as:

$$D_e = \frac{\epsilon_p D_{\text{macro}}}{\tau K} \tag{5.7}$$

Henry's Law constant for each temperature was obtained using the dual-site Langmuir fitted parameters. This will be explained in more detail in the next section. Tortuosity is a physical property of porous material, and it shows the deviation of the pores from an ideal cylindrical shape [12]. As a result, it does not depend on the system conditions such as temperature and the pressure. Prior to any analysis, the tortuosity value should be set for the activated carbon sample. Porosity and tortuosity of 2-GA activated carbon as obtained from mercury intrusion experiments were 0.33 and 2.1 respectively. Measured tortuosity value was lower than the reported values in the literature for activated carbons which are in the range of 3-9 [15, 24].

Table 5.4: Parameters and calculated values from ZLC desorption curves

Temperature [°C]	slope [1/s]	D_e/R^2 [1/s]	intercept [-]	L [-]
30	-0.024	0.0027	0.044	46.4
50	-0.047	0.0053	0.049	41.9
70	-0.091	0.0101	0.057	35.8

In order to set the tortuosity of the activated carbon sample, desorption rate at different temperatures were compared. Macropore diffusivity is a combination of molecular, Knudsen, surface, and viscous flow diffusions. Surface and viscous flow contributions are neglected in this study as discussed earlier in this section. According to the earlier experiments on different particle sizes of activated carbons, it was confirmed that macropore diffusion was the controlling mass transfer mechanism in the system under study. Therefore, desorption rate is controlled only by the combination of molecular and Knudsen diffusivities. In this analysis, tortuosity was fitted for each experiment separately, and the diffusivities were calculated by Chapman-Enskog equation combined in series with Knudsen Diffusivity [12]. Even though the proportion of macropores in the adsorption is negligible, their contribution in the diffusion is still important. According to section 4.7.2, the average pore size of the macropores was calculated to be 0.7 μm. This value was used in Knudsen diffusion calculation. In this pore size range the influence of molecular diffusion was more significant than that of Knudsen diffusion. Measured effective pore diffusivity (D_e) from ZLC experiments, calculated molecular diffusivity ($D_{m,cal}$), Knudsen diffusivity ($D_{K,cal}$), combined diffusivity ($D_{macro,cal}$), and the fitted tortuosity (τ) values for each temperature are summarized in Table 5.5.

As seen, the fitted values of tortuosity for the three experiments are close to each other with the average of 1.6. They are in the same range as the tortuosity measured by mercury intrusion porosimetry ($\tau = 2.1$). The same temperature dependence was also noticed by Da Silva and Rodrigue [60] while studying the kinetics of propane over 13X, where combination of molecular and Knudsen diffusion was considered as the controlling mechanisms. Consequently, surface diffusion is negligible compared to the gas phase flux in the pores,

Table 5.5: Predicted macropore diffusivities and the the values obtained from helium ZLC curves at different temperatures, 50 sccm flow rate

Temperature [°C]	$D_{m,cal}$ $[m^2/s]$	$D_{K,cal}$ $[m^2/s]$	$D_{macro,cal}$ $[m^2/s]$	D_e $[m^2/s]$	τ [-]
30	5.86×10^{-5}	2.16×10^{-4}	4.61×10^{-5}	4.4×10^{-9}	1.76
50	6.35×10^{-5}	2.23×10^{-4}	5.05×10^{-5}	8.7×10^{-9}	1.74
70	7.17×10^{-5}	2.29×10^{-4}	5.46×10^{-5}	1.7×10^{-8}	1.53

and the tortuosity of the sample is confirmed to be ~ 2.

Figure 5.11 illustrates the temperature dependence of the calculated and measured diffusivities. According to this figure, temperature dependence of measured diffusivity ($D_{\mathrm{e}}.K$) at the range under study is more noticeable than that of molecular and Knudsen diffusivities. However, the measured diffusivity is comparable with the molecular diffusivity for experiments at 30 and 50°C. Comparison is shown in Fig. 5.12. In this figure, y-axis is the normalized diffusivity and the x-axis is the temperature. Differences for the 70°C might be caused by the errors in the estimations of the slope of the long time asymptote and the equilibrium constant. Error analysis is explained in more details in Appendix A. In addition, gas diffusion is faster at higher temperatures which makes the measurement difficult. This introduces a limit for diffusivity measurement by ZLC technique [21].

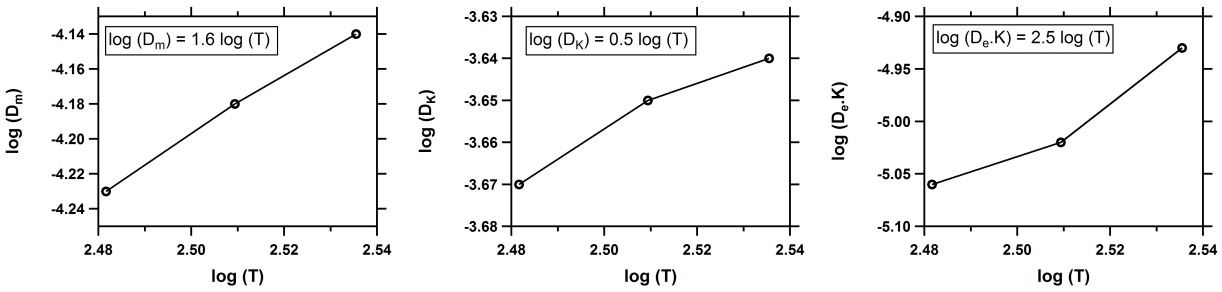

Figure 5.11: Temperature dependence of molecular, Knudsen and measured diffusivities.

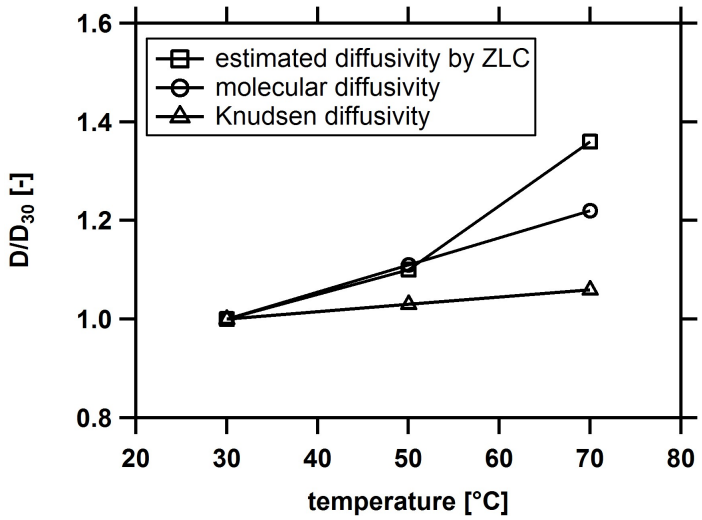

Figure 5.12: Comparison of temperature dependence of molecular, Knudsen and measured diffusivities.

Effective Henry's Law constant is generally calculated for each ZLC experiment using the intercept of long time asymptote as described in chapter 3. Figure 5.13 illustrates K values obtained from the intercept of ZLC experiments at 30°C for 10, 20, 30 and 50 sccm purge gas flow rates. According to this figure, Henry's constant depends on the purge gas flow rate; lower K values was obtained for higher flow rates. Hu et al. [39] have suggested to measure the effective Henry's Law constant by performing ZLC experiments at equilibrium conditions, when slope of desorption curve is directly proportional to K. These measurements have been described comprehensively by Brandani et al. [40]. In our measurements, even at flow rate of 10 sccm system was not under equilibrium conditions, as discussed in section 5.1.2. The alternative solution used in our calculations was to obtain the equilibrium constant using the dual-site Langmuir fitted parameters at each temperature. It is assumed that this value remains constant for all the flow rates. The predicted equilibrium constant for 30°C is shown by the dotted line in Fig. 5.13. It is expected at lower flow rates (equilibrium conditions) effective Henry's constant calculated by the ZLC desorption curves increases exponentially.

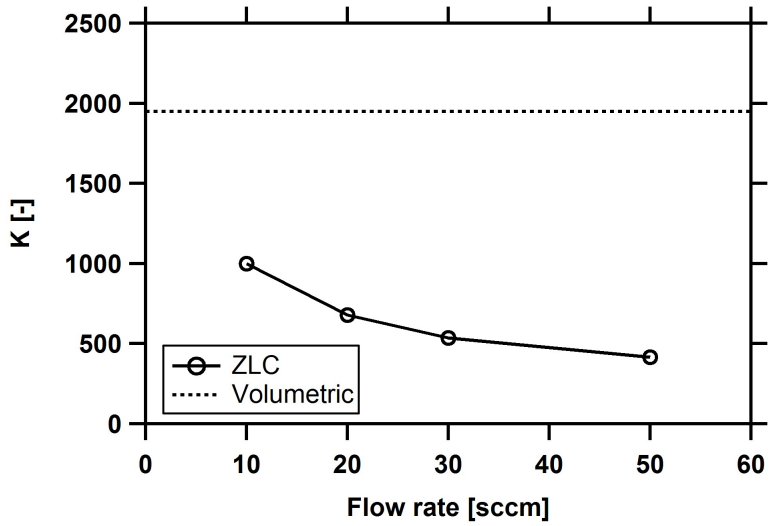

Figure 5.13: Comparison of experimental ZLC curves on activated carbon particle at 0.01 atm of ethane in two different purge gases (N_2 and He), 30°C and 50 sccm.

Experiments with nitrogen purge

According to Park et al. [58], activated carbons show adsorption capacity for nitrogen. Nitrogen loading at 1 bar partial pressure is approximately 0.25 $[\frac{mol}{kg}]$ half of ethane loading at 0.01 bar partial pressure on activated carbon. Therefore, competitive adsorption is expected for nitrogen experiments. This affects all the calculations. In order to consider the competition between ethane and nitrogen, Henry's Law constant for this system was calculated using reported single-site Langmuir parameters for nitrogen at 30°C by Park et al. [58] using below equation:

$$H_{\mathrm{C_2,mix}} = \frac{H_{\mathrm{C_2}}}{1 + b_{N2} C_{N2}} \tag{5.8}$$

where H_c is Henry's constant of ethane at presence of nitrogen, H is Henry's constant of ethane calculated by single component dual-site Langmuir parameters, b_{N2} is the affinity parameter for nitrogen in a single-component system, and C_{N2} is the concentration of nitrogen in the gas phase. Resulting Henry's constant was 1600 which is less than 1950, calculated from volumetric experiments. This confirms the competition effect as discussed above. It should be mentioned that the activated carbon sample used in [58] might be different in adsorption properties from the 2-GA sample used in this study. This changes

the estimated isotherm parameters of nitrogen. Thus, variations in calculated Henry's Law constant is expected. If competition effect is neglected in the calculation, there will be a discrepancy between the ZLC results and the predicted pore diffusivity. The results are summarized in Table 5.6. Obtained effective diffusivity from ZLC long time approach was 2 times faster than the predicted effective diffusivity calculated using the related equations and the fitted tortuosity (1.7). Further experiments on ethane desorption by nitrogen at different temperatures and concentrations are required to investigate dynamics of the system.

Table 5.6: Summary of values of diffusivity for nitrogen calculated and obtained from ZLC curves

$D_{\mathrm{m,cal}}$ $[m^2/s]$	$D_{\mathrm{K,cal}}$ $[m^2/s]$	$D_{\mathrm{e,cal}}$ $[m^2/s]$	$D_{\mathrm{e,\ exp}}$ $[m^2/s]$
1.61×10^{-5}	2.16×10^{-4}	1.7×10^{-9}	3.3×10^{-9}

5.2.3 Heterogeneity among the particles

Heterogeneity is expected among the activated carbon particles. In order to see this, ZLC experiments on one particle of 2-GA activated carbon (3.5 mg) were carried out. This new particle was similar in mass and shape to the older particle (3.7 mg) used for experiments with different purge gases and temperatures. The ZLC experiments were performed in the same sequence with the same regeneration and saturation steps. The comparison of the experimental results is shown in Fig 5.14. The long time asymptotes of these two samples show different behaviors. This indicates that the diffusion of C_2 in these two samples or the physical properties of the particles are different.

5.3 Summary

Isotherms of ethane on activated carbon sample were measured and fitted using volumetric experiments. In the next step, kinetics of dilute ethane in activated carbon was studies

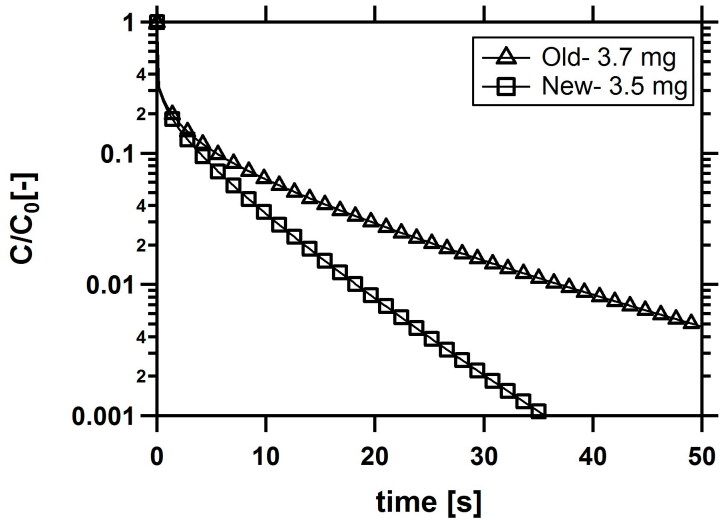

Figure 5.14: Comparison of ZLC desorption curves for old (3.7 mg) and new (new) particles.

using ZLC experiments. Several configurations were tested in order to break down the different possible mechanisms. Experiments for various particle sizes showed that desorption rate in the system under study, was controlled by gas diffusion in the macropores. Another experimental confirmation for macropore diffusion was obtained by changing the purge gas type. In addition, experiments at different temperatures were performed in order to fit tortuosity of the adsorbent. The measured values obtained from the ZLC experiments were aligned with the predicted parameters from available equations and solid properties.

Chapter 6

Conclusions and Recommendations

This study was focused on determination of diffusion in porous materials using the ZLC method. The main advantages and limitations of this approach have been noted in chapters 3 and 5. This information is summarized in this chapter.

In the present work, diffusion measurements of dilute ethane on 2-GA activated carbon particles manufactured by Kuraray Co. were completed. Solid characterization measurements were performed using mercury intrusion porosimetry and N_2 adsorption techniques prior to the ZLC experiments. Physical properties of the adsorbent sample were analyzed. Pore size distribution, porosity, and tortuosity of the sample were determined and compared to the values reported in the literature. Isotherms of ethane on activated carbon at different temperatures were measured using volumetric method, and the dual-site Langmuir parameters were fitted to the experimental data using non-linear regression. The ZLC set-up was built during the course of this project. Flame ionization detector was used as the sensitive detector connected to the outlet of the ZLC set-up, in order to monitor the concentration of ethane in the effluent gas. Dead volume measurements resulted the value of 0.5 cc, which is comparable to data published in the literature. ZLC method depends on following the desorption curve measured at sufficiently high flow rates when system is under non-equilibrium conditions, and desorption rate is controlled by diffusion.

The experiments provided useful methods for studying the diffusion mechanism of the test gas in the adsorbent particles. Experimental results i.e. Ft plots indicated that under the studied conditions, desorption rate was controlled by diffusion of gas out of adsorbent particles. Different particle sizes of the activated carbon were tested, in order to verify the diffusion mechanism. The experimental results were affected by the particle sizes. This confirms macropore diffusion in the system under study. Surface diffusion was neglected in this study because the ZLC experiments were performed at very low surface coverage. Also, viscous flow diffusion was overpassed, due to insignificant pressure drop across the adsorbent particle. According to the experiments on different purge gas types, it was observed that the desorption rates were dependent on the nature of the purge gas. Diffusional time constants for nitrogen were slower than helium. This is related to different interactions that are between molecules in ethane/helium and ethane/nitrogen mixtures. Therefore, macropore diffusion was assumed to be the contribution of molecular and Knudsen diffusivities. There was a good agreement between the calculated diffusivities from equations, solid properties obtained from characterization tests and the ZLC experiments.

6.1 Recommendations

ZLC measurements were carried out on one particle of the adsorbent. However, activated carbons have shown heterogeneity within the sample batch. Therefore, it is recommended to study adsorption/desorption characteristics in such systems on bulk amounts of the sample. If the aim is to understand the diffusion mechanisms, ZLC technique will be a suitable candidate, providing reliable estimation of the diffusivity values. Another limitation in the present study was the equilibrium measurements. Due to the flow controllers used in the current ZLC set-up, equilibrium conditions were not achievable to collect isotherm data. It is recommended for the future works to study equilibrium measurements on ZLC prior to diffusion experiments using suitable flow controllers. Furthermore, in order to avoid trace amounts of water in the cylinders, it is suggested to add drying columns downstream of the gas cylinders. This enhances the measured capacity of ad-

sorbent in ZLC experiments. In order to observe the contribution of surface diffusion to the total desorption rate, ZLC experiments at higher concentrations of ethane can be performed. This can be achieve by adding an ethane stream to the test line before the main switching valve, in order to attain concentrated gas. It is recommended to perform the experiments differentially to study the concentration dependence of surface diffusion in the system under study.

The diffusivity value obtained from ZLC experiment for nitrogen purge, was not fully in line with the predicted diffusivities using the related equations. It was approximately two times faster than that of the combination of molecular and Knudsen for ethane/nitrogen mixture. It may be caused by competition between nitrogen and ethane. It is suggested to measure nitrogen isotherms of the activated carbon sample at different temperatures, and perform ZLC experiments using nitrogen purge at those temperatures. Therefore, the comparison between the experimental results and predicted diffusivities develops a better understanding of the system. Experiments on dilute ethane in nitrogen carrier gas and different purge gases will also provide good insight to the matter, and will show the effect of carrier gas in the experiments.

Bibliography

[1] Q. Wang, X. Chen, A. N. Jha, and H. Rogers, "Natural Gas from Shale Formation The Evolution, Evidences and Challenges of Shale Gas Revolution in United States," *Renewable Sustainable Energy Rev.*, vol. 30, pp. 1–28, 2014.

[2] Internatinal Energy Agency, *OECD/IEA 2016 Key Natural Gas Trends*. IEA Publishing, 2016.

[3] The Alberta Energy Resources Conservation Board, *Alberta's Energy Industry an Overview*. Government of Alberta, 2012.

[4] Gas Processors Association Board of Authors, *11th Edition GPSA Engineering Data Book*. Gas Processors Suppliers Association, 1998.

[5] S. Thomas, "Enhanced Oil Recovery-an Overview," *Oil Gas Sci. Technol.*, vol. 63, pp. 9–19, 2008.

[6] M. Huff and L. D. Schmidt, "Ethylene Formation by Oxidative Dehydrogenation of Ethane Over Monoliths at Very Short Contact Times," *J. Phys. Chem.*, vol. 97, pp. 11815–11822, 1993.

[7] M. Arruebo, J. Coronas, M. Menendez, and J. Santamarıa, "Separation of Hydrocarbons from Natural Gas Using Silicalite Membranes," *Sep. Purif. Technol.*, vol. 25, pp. 275–286, 2001.

[8] N. Magnowski, A. Avila, C. Lin, M. Shi, and S. Kuznicki, "Extraction of Ethane from Natural Gas by Adsorption on Modified ETS-10," *Chem. Eng. Sci.*, vol. 66, pp. 1697–1701, 2011.

[9] L. E. Perez, A. M. Avila, J. A. Sawada, A. Rajendran, and S. M. Kuznicki, "Process Optimization-Based Adsorbent Selection for Ethane Recovery from Residue Gas," *Sep. Purif. Technol.*, vol. 168, pp. 19–31, 2016.

[10] A. Malek and S. Farooq, "Kinetics of Hydrocarbon Adsorption on Activated Carbon and Silica Gel," *AIChE J.*, vol. 43, pp. 761–776, 1997.

[11] A. Malek and S. Farooq, "Determination of Equilibrium Isotherms Using Dynamic Column Breakthrough and Constant Flow Equilibrium Desorption," *J. Chem. Eng. Data*, vol. 41, pp. 25–32, 1996.

[12] D. Ruthven, *Principles of Adsorption and Adsorption Processes*. Wiley, 1984.

[13] R. T. Yang, *Gas Separation by Adsorption Processes*. Butterworths, 1987.

[14] M. Eic and D. M. Ruthven, "A New Experimental Technique for Measurement of Intracrystalline Diffusivity," *Zeolites*, vol. 8, pp. 40–45, 1988.

[15] P. Mayfield and D. Do, "Measurement of the Single-Component Adsorption Kinetics of Ethane, Butane and Pentane onto Activated Carbon Using a Differential Adsorption Bed," *Ind. Eng. Chem. Res.*, 1991.

[16] R. Bansal, *Activated Carbon Adsorption*. Taylor & Francis, 2005.

[17] M. Thommes, K. Kaneko, A. V. Neimark, J. P. Olivier, F. Rodriguez-Reinoso, J. Rouquerol, and K. S. Sing, "Physisorption of Gases, with Special Reference to the Evaluation of Surface Area and Pore Size Distribution (IUPAC Technical Report)," *Pure Appl. Chem.*, vol. 87, pp. 1051–1069, 2015.

[18] H. Giesche, "Mercury Porosimetry: a General (Practical) Overview," *Part. Part. Syst. Char.*, vol. 23, pp. 9–19, 2006.

[19] L. E. Perez, "Ethane Recovery from Residue Gas Using Pressure Swing Adsorption," Master's thesis, University of Alberta, 2015.

[20] S. A. Hosseinzadeh Hejazi, A. Rajendran, J. A. Sawada, and S. M. Kuznicki, "Dynamic Column Breakthrough and Process Studies of High-Purity Oxygen Production Using Silver Exchanged Titanosilicates (Ag-ETS-10)," *Ind. Eng. Chem. Res.*, vol. 55, p. 59936005, 2016.

[21] J. Karger, D. M. Ruthven, and D. N. Theodorou, *Diffusion in Nanoporous Materials*. Wiley-VCH, 2012.

[22] R. Bird, W. Stewart, and E. Lightfoot, *Transport Phenomena*. J. Wiley, 2002.

[23] S. Sircar, T. Golden, and M. Rao, "Activated Carbon for Gas Separation and Storage," *Carbon*, vol. 34, pp. 1–12, 1996.

[24] P. Gray and D. Do, "Adsorption and Desorption of Gaseous Sorbates on a Bidispersed Particle with Freundlich Isotherm: II. Experimental Study of Sulphur Dioxide Sorption on Activated Carbon Particles," *Gas Sep. Purif.*, vol. 3, pp. 201–208, 1989.

[25] I. Neretnieks, "Analysis of Some Adsorption Experiments with Activated Carbon," *Chem. Eng. Sci.*, vol. 31, pp. 1029–1035, 1976.

[26] P. G. Gray and D. D. Do, "Dynamics of Carbon Dioxide Sorption on Activated-Carbon Particles," *AIChE J.*, vol. 37, pp. 1027–1034, 1991.

[27] S.-J. Doong and R. Yang, "Bulk Separation of Multicomponent Gas Mixtures by Pressure Swing Adsorption: Pore/Surface Diffusion and Equilibrium Models," *AIChE J.*, vol. 32, pp. 397–410, 1986.

[28] D. Do, X. Hu, and P. Mayfield, "Multicomponent Adsorption of Ethane, n-butane and n-pentane in activated carbon," *Gas Sep. Purif.*, vol. 5, pp. 35–48, 1991.

[29] A. Kapoor, R. T. Yang, and C. Wong, "Surface Diffusion," *Catalysis Reviews*, vol. 31, pp. 129–214, 1989.

[30] S. Bhatia and D. Do, "On the Concentration Dependence of Surface Diffusion Coefficients in Capillary Porous Materials," in *Proceedings of the Royal Society of London A: Mathematical, Physical and Engineering Sciences*, vol. 434, 1991.

[31] D. D. Do, "A Model for Surface dDiffusion of Ethane and propane in Activated Carbon," *Chem. Eng. Sci.*, vol. 51, pp. 4145–4158, 1996.

[32] X. Hu, D. Do, and G. Rao, "Experimental Concentration Dependence of Surface Diffusivity of Hydrocarbons in Activated Carbon," *Chem. Eng. Sci.*, vol. 49, pp. 2145–2152, 1994.

[33] X. Hu and D. D. Do, "Multicomponent Adsorption Kinetics of Hydrocarbons onto Activated Carbon: Contribution of Micropore Resistance," *Chem. Eng. Sci.*, vol. 48, pp. 1317–1323, 1993.

[34] X. Hu, S. Brandani, A. I. Benin, and R. R. Willis, "Development of a Semiautomated Zero Zength Column Technique for Carbon Capture Applications: Study of Diffusion Behavior of CO_2 in MOFs," *Ind. Eng. Chem. Res.*, vol. 54, pp. 5777–5783, 2015.

[35] X. Hu, S. Brandani, A. I. Benin, and R. R. Willis, "Development of a Semiautomated Zero Length Column Technique for Carbon Capture Applications: Rapid Capacity Ranking of Novel Adsorbents," *Ind. Eng. Chem. Res.*, vol. 54, pp. 6772–6780, 2015.

[36] J. A. Silva, F. A. Da Silva, and A. E. Rodrigues, "An Analytical Solution for the Analysis of Zero-Length-Column Experiments with Heat Effects," *Ind. Eng. Chem. Res.*, vol. 40, no. 16, pp. 3697–3702, 2001.

[37] W. Duncan and K. Möller, "A zero lengthcriterion for ZLC chromatography," *Chem. Eng. Sci.*, vol. 55, no. 22, pp. 5415–5420, 2000.

[38] F. Brandani, *Development and Application of the Zero Length Column (ZLC) Techique for Measuring Adsorption Equilibria*. PhD thesis, University of Maine, 2002.

[39] X. Hu, E. Mangano, D. Friedrich, H. Ahn, and S. Brandani, "Diffusion Mechanism of CO_2 in 13X Zeolite Beads," *Adsorption*, vol. 20, pp. 121–135, 2014.

[40] F. Brandani, D. Ruthven, and C. G. Coe, "Measurement of Adsorption Equilibrium by the Zero Length Column (ZLC) Technique Part 1: Single-Component Systems," *Ind. Eng. Chem. Res.*, vol. 42, pp. 1451–1461, 2003.

[41] F. Brandani and D. Ruthven, "Measurement of Adsorption Equilibria by the Zero Length Column (ZLC) Technique Part 2: Binary Systems," *Ind. Eng. Chem. Res.*, vol. 42, pp. 1462–1469, 2003.

[42] S. Brandani, "A Simple Graphical Check of Consistency for Zero Length Column Desorption Curves," *Chem. Eng. Technol.*, vol. 39, pp. 1194–1198, 2016.

[43] D. M. Ruthven and Z. Xu, "Diffusion of Oxygen and Nitrogen in 5A Zeolite Crystals and Commercial 5A Pellets," *Chem. Eng. Sci.*, vol. 48, pp. 3307–3312, 1993.

[44] A. Vidoni and D. M. Ruthven, "Diffusion of C_2H_6 and C_2H_4 in DDR Zeolite," *Ind. Eng. Chem. Res.*, vol. 51, pp. 1383–1390, 2012.

[45] S. Brandani, J. Hufton, and D. Ruthven, "Self-Diffusion of Propane and Propylene in 5A and 13X zeolite Crystals Studied by the Tracer ZLC Method," *Zeolites*, vol. 15, pp. 624–631, 1995.

[46] D. M. Ruthven and P. Stapleton, "Measurement of Liquid Phase Counter-Diffusion in Zeolite Crystals by the ZLC Method," *Chem. Eng. Sci.*, vol. 48, pp. 89–98, 1993.

[47] S. Brandani, "Effects of Nonlinear Equilibrium on Zero Length Column Experiments," *Chem. Eng. Sci.*, vol. 53, pp. 2791–2798, 1998.

[48] S. Brandani, C. Cavalcante, A. Guimarães, and D. Ruthven, "Heat Effects in ZLC Experiments," *Adsorption*, vol. 4, pp. 275–285, 1998.

[49] S. Brandani, "Analytical Solution for ZLC Desorption Curves with Bi-porous Adsorbent Particles," *Chem. Eng. Sci.*, vol. 51, pp. 3283–3288, 1996.

[50] S. Brandani and D. M. Ruthven, "Analysis of ZLC Desorption Curves for Liquid Systems," *Chem. Eng. Sci.*, 1995.

[51] S. Brandani, M. A. Jama, and D. M. Ruthven, "Zlc Measurements under Non-linear Conditions," *Chem. Eng. Sci.*, vol. 55, pp. 1205–1212, 2000.

[52] J. A. Silva, K. Schumann, and A. E. Rodrigues, "Sorption and Kinetics of CO_2 and CH_4 in Binderless Beads of 13X Zeolite," *Microporous Mesoporous Mater.*, vol. 158, pp. 219–228, 2012.

[53] O. Auban, J. Malet, P. Brun, J. Brinster, J. Quillico, and E. Studer, "Implementation of Gas Concentration Measurement Systems Using Mass Spectrometry inContainment Thermal-Hydraulics Test Facilities: Different Approaches for Calibration and Measurement with Steam/Air/Helium Mixtures," in *10th International Topical Meeting on Nuclear Reactor Thermal Hydraulics (NURETH-10), Seoul, Korea*, 2003.

[54] P. A. Webb, "An Introduction to the Physical Characterization of Materials by Mercury Intrusion Porosimetry with Emphasis on Reduction and Presentation of Experimental Data," *Micromeritics Instrument Corp, Norcross, Georgia*, 2001.

[55] K. Sing, "The Use of Nitrogen Adsorption for the Characterisation of Porous Materials," *Colloids Surf., A*, vol. 187, pp. 3–9, 2001.

[56] S. Brunauer, P. H. Emmett, and E. Teller, "Adsorption of Gases in Multimolecular Layers," *J. Am. Chem. Soc.*, vol. 60, pp. 309–319, 1938.

[57] J. De Boer, B. Linsen, and T. J. Osinga, "Studies on Pore Systems in Catalysts: VI. The Universal t Curve," *J. Catal.*, vol. 4, pp. 643–648, 1965.

[58] Y. Park, D.-K. Moon, Y.-H. Kim, H. Ahn, and C.-H. Lee, "Adsorption Isotherms of CO_2, CO, N_2, CH_4, Ar and H_2 on Activated Carbon and Zeolite LiX up to 1.0 MPa," *Adsorption*, vol. 20, pp. 631–647, 2014.

[59] H. Do and D. Do, "Maxwell-Stefan Analysis of Multicomponent Transient Diffusion in a Capillary and Adsorption of Hydrocarbons in Activated Carbon Particle," *Chem. Eng. Sci.*, vol. 53, pp. 1239–1252, 1998.

[60] F. A. Da Silva and A. E. Rodrigues, "Adsorption Equilibria and Kinetics for Propylene and Propane over 13X and 4A Zeolite Pellets," *Ind. Eng. Chem. Res.*, vol. 38, pp. 2051–2057, 1999.

Appendix A

Error Analysis

Slopes and the intercepts of ZLC experiments are calculated at very low concentrations (below 0.01%), but they are sensitive to the time range that the asymptote is considered (Fig. A.1). Different asymptotes result in various intercept and slope values which indicate non-equal pore diffusivities. This has a major effect on the intercept of the $ln(\frac{c}{c_0})$ versus t plot and minor on the slope and the diffusional time constant. According to Fig. A.1, calculated L values for the three intercepts vary from 39 to 55, and diffusional time constants change from 0.0026 to 0.0028. Therefore, variations in L directly affects

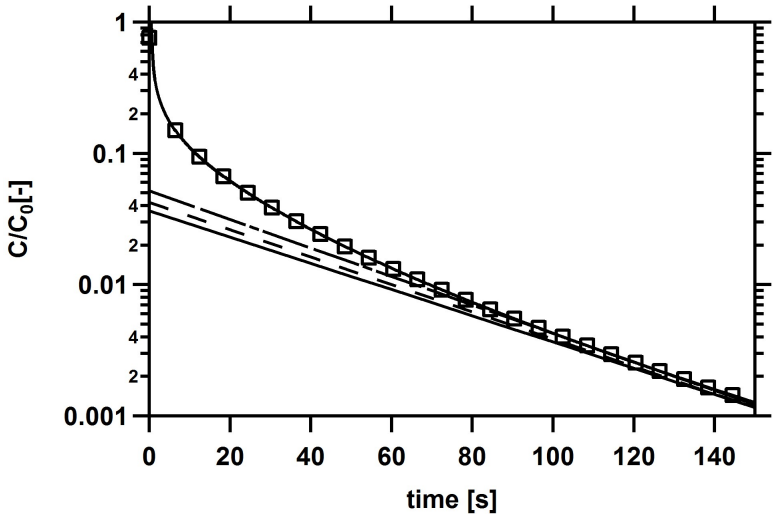

Figure A.1: Demonstration of various asymptotic approaches on the ZLC desorption curves.

the calculated pore diffusivity. In order to eliminate this, Henry's Law constants were calculated using the fitted parameters for the volumetric equilibrium measurements. It is worthwhile to remind that the measured loadings using ZLC experiments are lower than those predicted from volumetric method. Uncertainty in the calculated pore diffusivity is expected, as caused by the variations in the slope of the ZLC asymptote and the considered equilibrium constant. The expected uncertainty is calculated according to Eq. A.1, where ΔD_e is the variations of the effective diffusivity and ΔK is the expected uncertainty in effective Henry's constant. Effective pore diffusivity variation is approximately 1×10^{-6}. This will change the fitted tortuosity in the range of 2.5 to 1.5.

$$\Delta D_{\text{macro}} = ((\frac{\partial D_{\text{macro}}}{\partial D_e}\Delta D_e)^2 + (\frac{\partial D_{\text{macro}}}{\partial K}\Delta K)^2)^{0.5} \tag{A.1}$$

Appendix B

ZLC Experimental Data Reproducibility and Repeatability

As stated in the ZLC results section, ZLC experiments for each condition were performed couple of times. The comparison between the repeated tests are shown in this section.

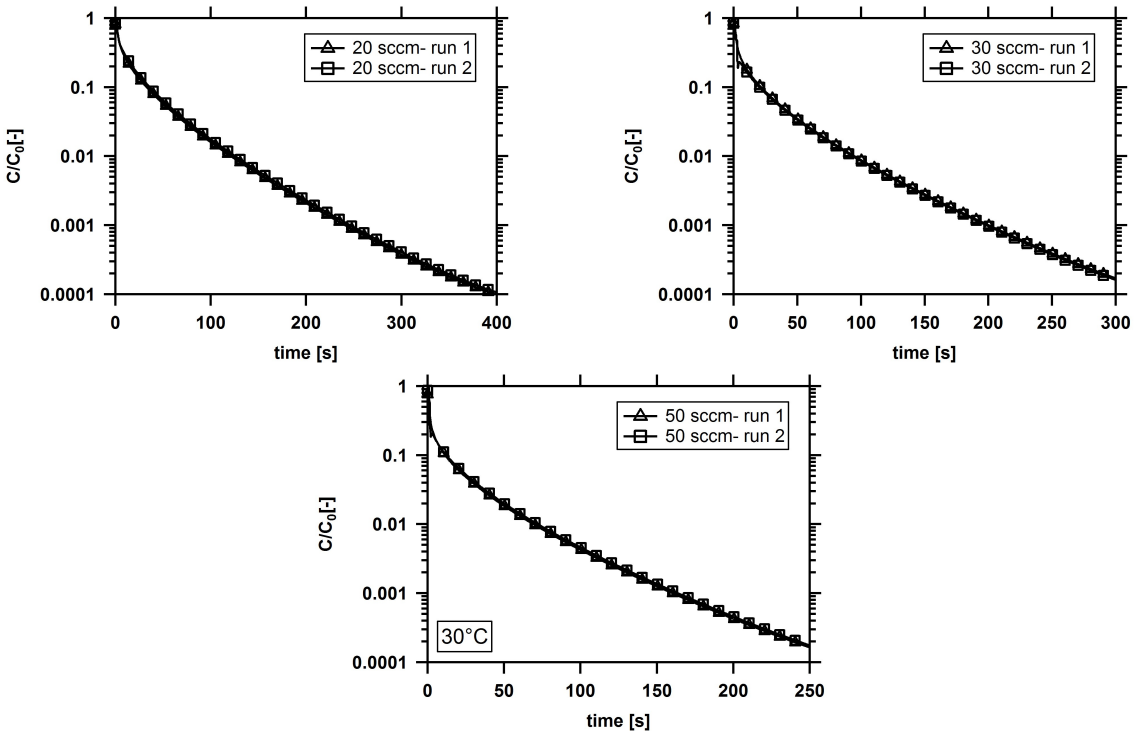

Figure B.1: Experimental ZLC response curves of Activated carbon at 0.01 atm of ethane at 30°C, purging with helium at 20, 30 and 50 sccm.

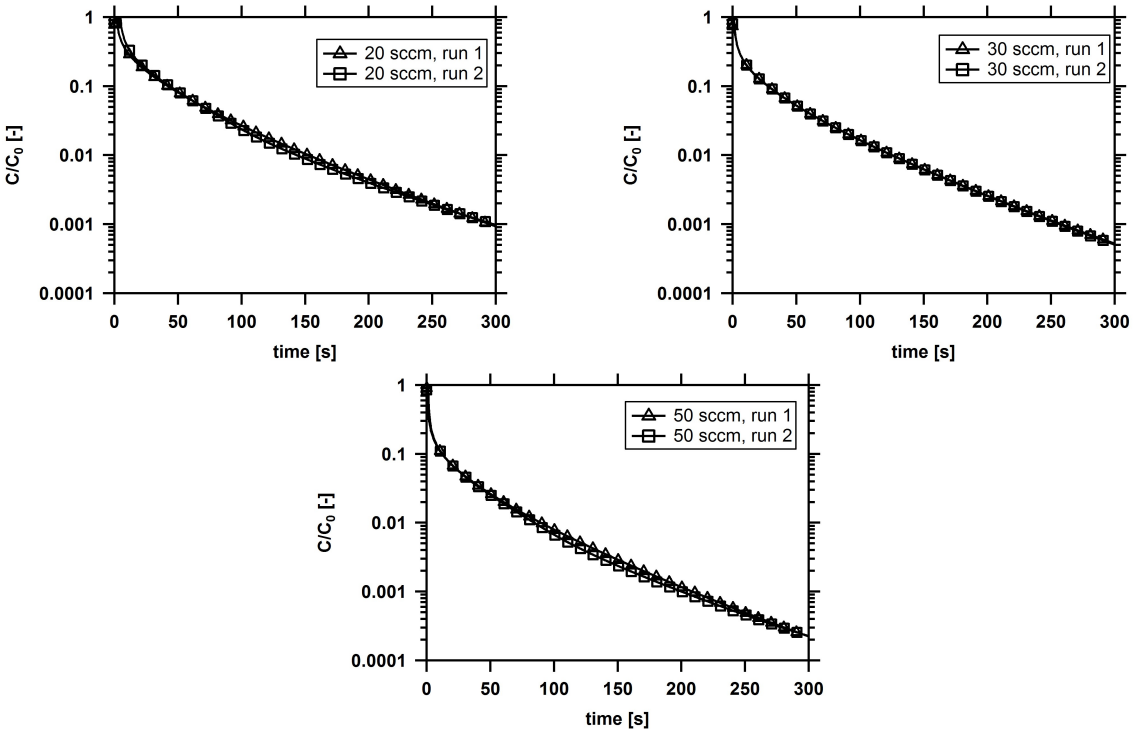

Figure B.2: Experimental ZLC response curves of Activated carbon at 0.01 atm of ethane at 30°C, purging with nitrogen at 20, 30 and 50 sccm.

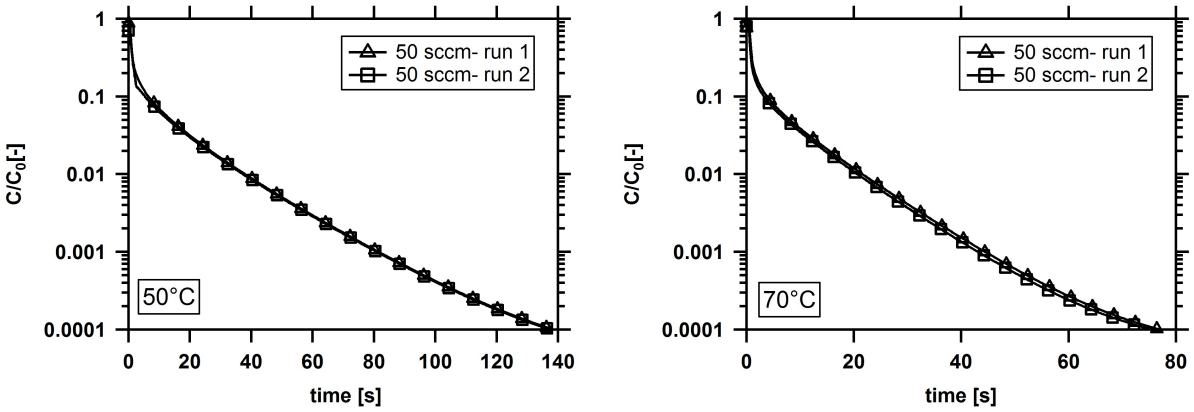

Figure B.3: Experimental ZLC response curves of Activated carbon at 0.01 atm of ethane at 50° and 70°C, purging with helium at 50 sccm.